GeoArabia, 2014, v. 19, no. 4, p. 113-140
Gulf PetroLink, Bahrain

Open *versus* closed mesogenetic systems in Cretaceous fluvial and tidal sandstones, Sirt Basin, Libya

Muftah Khalifa and Marta Gasparrini

ABSTRACT

This study constrains factors controlling the distribution of diagenetic alteration and their impact on reservoir quality of the Cretaceous sandstones from the Al-Bayda Platform, located in the southern Sirt Basin (Libya). These factors include the presence of early cements as well as the influx of hot basinal brines. The studied samples come from two blocks in the Khalifa Field, which are dislocated by a major normal fault. The deep-burial (mesogenetic) alteration includes the partial to pervasive replacement of early (eogenetic) dolomite and calcite cements by ferroan-dolomite, ankerite and siderite, precipitation of grain-coating chlorite, and cementation by quartz overgrowths, barite and anhydrite, particularly in the downthrown block. The association of quartz overgrowths with barite suggests that deep burial was influenced by the influx of hot basinal brines through faults. Conversely, deep-burial alteration in braided fluvial deposits of the Nubian sandstones of the upthrown block include: illitization of eogenetic smectite, quartz cementation and formation of chlorite.

This study shows that deep burial of the studied sandstones did not occur in a closed system, but was affected by the influx of hot basinal brines through faults, which formed during basin rifting. This interpretation is supported by the relatively high homogenization temperatures (100–110°C; corrected to 110–125°C) of primary fluid inclusions within quartz overgrowths, which exceed the maximum burial temperatures experienced by the Cretaceous succession, and by the high salinity of these inclusions.

INTRODUCTION

Diagenesis may account for post-depositional porosity modification and evolution in three different realms or zones (e.g. eogenetic, mesogenetic and telogenetic) which were first recognized for carbonates by Choquette and Pray (1970), and later largely applied to siliciclastics (e.g. Morad et al., 2000; Worden and Burley, 2003). These realms or zones and associated diagenetic processes roughly correspond with temporal stages: (1) Eogenesis (early diagenetic alteration) includes all processes that occur at or near the sedimentation surface, where the chemistry of the interstitial waters is controlled mainly by the depositional environments and paleoclimatic conditions (Berner, 1980; De Ros et al., 1994; Morad et al., 2000; Morad et al., 2010); (2) Mesogenesis (deep-burial alteration) acts during sediment burial and includes all the diagenetic processes that occur once the sediment has passed from the influence of the depositional environment and before the onset of the earliest stages of low-grade metamorphism (De Ros et al., 1994; Morad et al., 2000; Morad et al., 2010). Deep-burial alteration is controlled by basin thermal history, formation water chemistry, distribution of eogenetic alteration, and in some cases by fluxes of hydrothermal waters, in thermal disequilibrium with the ambient rocks (Gaupp et al., 1993; Worden and Morad, 2000; Ochoa et al., 2007); and (3) Telogenesis (exhumation alteration) occurs during or after uplift and erosion of previously buried sediments, commonly exposed to fluxes of meteoric waters (Bjørkum et al., 1990; Morad et al., 2000; Worden and Morad, 2003).

There is a strong controversy in literature regarding whether deep burial of sandstones occurs in open or closed systems (Bjørkum and Gjelsvik, 1988; Morad et al., 2000; Worden and Barclay, 2000). Some authors suggested that deep-burial alteration occurs in open systems (Hurst and Irwin, 1982; Berger et al., 1997; Land et al., 1997), in which mass transfer takes place by large-scale cross-formational flows of solutions (Glassman, 1992; Berger et al., 1997), which may be derived from adjacent mudstone

successions (Evans, 1989; Milliken et al., 1994; Land et al., 1997; Thyne, 2001). Some other authors suggested the role of fluxes of hot basinal brines through faults (Sullivan et al., 1990; Burley, 1993; Knipe, 1993; Morad et al., 1994; De Ros et al., 2000; Hendry et al., 2000; Ochoa et al., 2007; Wendte et al., 2009). Conversely, other authors suggested that deep-burial alteration in sandstones occurs mainly by small-scale diffusion in closed systems (Bjørkum and Gjelsvik, 1988; Giles et al., 1992; Bjørlykke, 1998; Worden et al., 1998).

In closed mesogenetic systems, the released ions are possibly re-precipitated as cements (Bjørkum and Gjelsvik, 1988), whereas in open mesogenetic systems fluxes of hot basinal brines through faults may carry the components needed for cementation (Burley et al., 1989; Knipe, 1993; Morad, et al., 1994; Walderhaug, 2000; Ochoa et al., 2007; Wendte et al., 2009). Deep hot basinal brines are reported to be rich in Si, Ba, Fe and Mg ions (Boles and Franks, 1979; Land and Fisher, 1987; Morad et al., 1994), which may precipitate as quartz, barite and siderite cements (Rossi et al., 2002).

The Cretaceous sandstones of the Nubian and Bahi formations are major reservoirs in the Sirt Basin (Libya). In the Khalifa Field, located on the Al-Bayda Platform in the southern Sirt Basin, the sandstones are offset by a major normal fault. The sandstones from the downthrown block display lower reservoir quality compared to the upthrown block, and this reservoir heterogeneity is attributed in this study to the occurrence and distribution of early and deep-burial (eo- and mesogenetic) alteration.

This study provides evidence that deep-burial (mesogenetic) alteration, which was enhanced by the influx of hot brines along faults, has affected considerably the reservoir quality of the Cretaceous Nubian and Bahi sandstones from the Al-Bayda Platform. The alteration has occurred in both open and closed diagenetic systems at different stages of the basin burial history. The results may help in predicting the spatial and temporal distribution of heterogeneities controlled by mesogenetic processes in similar siliciclastic reservoirs, which experienced a comparable burial evolution. This study follows on previous work by Khalifa and Morad (2012), which addressed the impact of structural setting on the diagenesis of Cretaceous sandstones in the Sirt Basin.

GEOLOGICAL SETTING OF THE SIRT BASIN

The Sirt Basin in northern Libya (Figure 1) is considered as a continental rift, belonging to the Tethyan rift system (Guiraud and Bosworth, 1997). The structural and stratigraphic evolution of the basin includes multiple tectonic phases: (1) intracontinental rifting, which may have continued from Late Carboniferous to Early Jurassic time (Van Houten, 1983); (2) initiation of the Sirt Basin as a result of extension during Jurassic–Tertiary time (Van Houten, 1980); and (3) re-activation of rifting during Tertiary time (Van der Meer and Cloetingh, 1996). The late Cretaceous rifting led to the collapse of the Tibesti-Sirt Arch into a series of NW-SE trending troughs and platforms during the Aptian (Finetti, 1982; Hallett and El-Ghoul, 1996). As a result, a triple junction formed between the Sirt arm (NW-SE trending), the Sarir-Hameimat arm (E-W trending), and Abu-Tumayam-Tibesti arm (NE-SW trending) (Harding, 1984; Ambrose, 2000; Ahlbrandt, 2001) (Figure 1a). The widespread volcanism (Al-Haruj Al-Swda) present in the southwestern part of the basin was related to the drift of the African plate over a fixed mantle hot spot during the Early Cretaceous (Van Houten, 1983).

The Sirt arm is dominated by normal faults and consists of a series of sub-parallel horsts and grabens, forming eastward tilted fault blocks oriented parallel to the rift axis. The structures are accompanied by E-W trending dextral shear zones, which run parallel to the structural strike of the Sarir-Hameimat arm (Finetti, 1982). The northwestern part of the Sirt Basin is dominated by NW- trending normal faults (Morley et al., 1990), whereas the southern and southeastern parts are dominated by E-ESE- trending faults.

The rift infill consists of basal continental to marine siliciclastics of Triassic, Late Jurassic and Cretaceous age, as well as marine carbonates and evaporites of Late Cretaceous and Tertiary (Paleocene, Miocene, and Plio-Pleistocene) age. The entire sequence is capped by Pleistocene and Holocene continental siliciclastics (Van der Meer and Cloetingh, 1996).

The Al-Bayda Platform (Figure 1b) is one of the platforms which make up the Sirt Basin. It is separated from the Az-Zahrah Platform by the narrow NNE trending Al-Kotlah Graben to the north, and bound

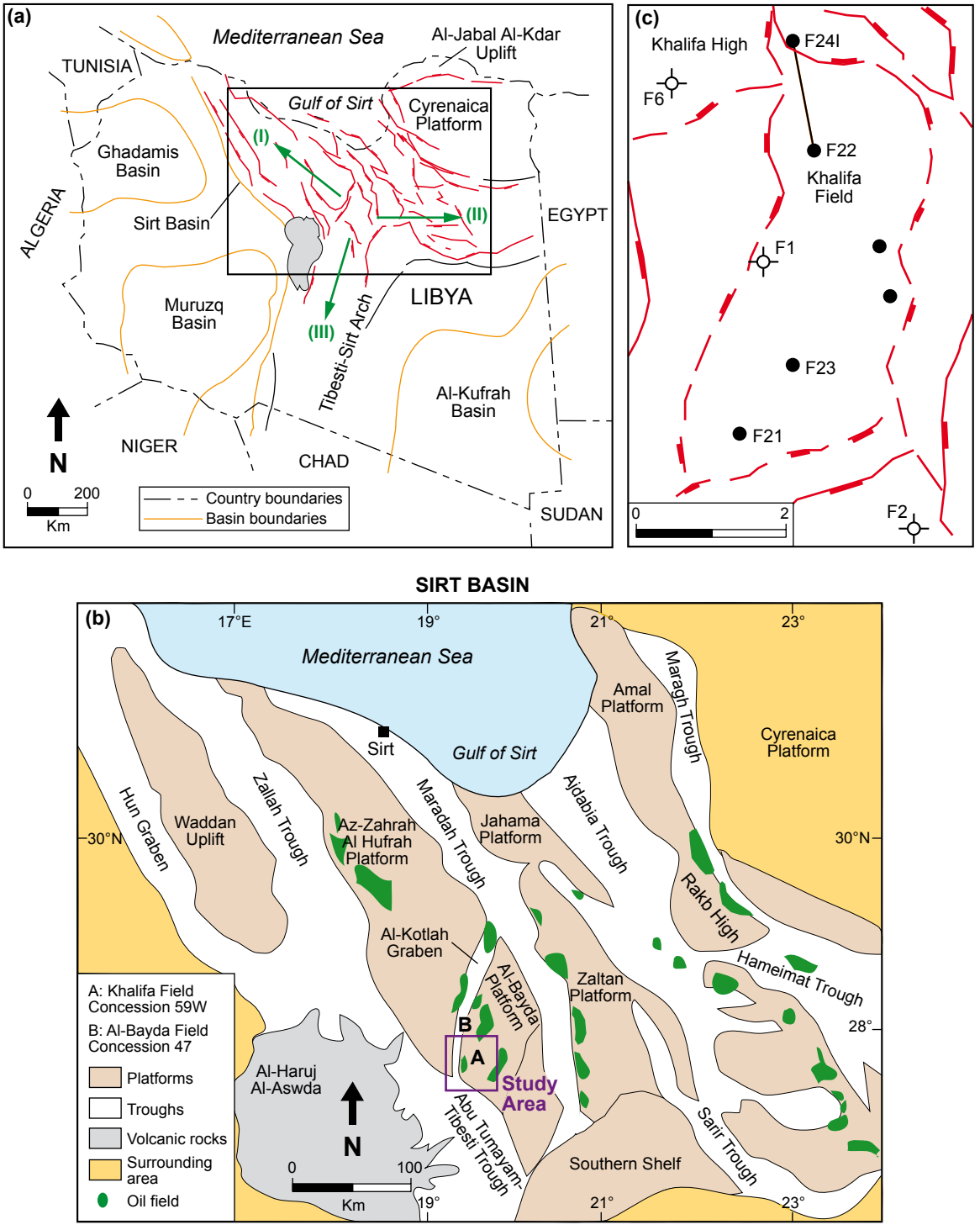

Figure 1: (a) Location map of the Sirt Basin showing the triple junction arms (green arrows): (I) the Sirt arm (NW-SE trending); (II) the Sarir-Hameimat arm (E-W trending); and (III) the Abu-Tumayam arm (NE-SW trending) (modified after Harding, 1984; Ambrose, 2000; Ahlbrandt, 2001). (b) Structural elements of the Sirt Basin, showing the location of the Al-Bayda Platform and the Khalifa Field study area (purple frame) including (c) a closer view on the location of the studied wells (F24I and F22).

by the Maradah Trough to the east, by the Zallah Trough to the west and by the Abu Tumayam-Tibesti Trough to the southwest (Van der Meer and Cloetingh, 1996). Sinha and Mriheel (1996) concluded that the southern part of the Al-Bayda Platform does not end abruptly along a faulted margin, but merges southwards across a shallow saddle with the Southern Shelf (Figure 1b). The platform was tilted ESE towards the Maradah Trough during Late Paleocene to Eocene (Schröter, 1996; Van der Meer and Cloetingh, 1996), combined by extensional fault re-activation (Anketell, 1996). The platform was partially transgressed during the Cenomanian, and progressively submerged during the Late Cretaceous (Ahlbrandt, 2001).

PETROLEUM GEOLOGY OF THE SIRT BASIN

The Sirt Basin ranks 13th among the world's petroleum provinces, having proven oil reserves estimated at 43.1 billion barrels of oil and 37.7 trillion cubic feet of natural gas (Petroconsultants, 1996; Ahlbrandt, 2001). The complex tectonic history of the Sirt Basin resulted in multiple reservoirs and conditions that favored hydrocarbon generation, migration, and accumulation principally on or adjacent to horst blocks (Price, 1980). Two major source rocks have been identified in the basin, including the Campanian–Turonian Sirte Shale, and the Paleocene Hagfa Shale (Magoon and Dow, 1994; El-Alami, 1996). The Sirte Shale charged Cambro–Ordovician and Cretaceous clastic reservoirs, as well as Late Cretaceous carbonate reservoirs, whereas the Hagfa Shale charged most of the Tertiary reservoirs. Other potential source rocks are the Lower Nubian Variegated Shale of Triassic–Lower Cretaceous age and the Paleocene Harash Formation (El-Alami, 1996).

The Sirte Shale ranges in thickness from a few hundred to more than 700 m in the troughs, and from few tens to few hundred meters on the horsts (Hallett, 2002). In some parts of the basin these source rocks are within the oil-generation window at depths of 2,700 to 3,400 m (Futyan and Jawzi, 1996). The Sirte Shale oil is characterized by low sulfur (0.3%) and relatively high gravity (average 36 API) (Petroconsultants, 1996). On the other hand, the Hagfa Shale is at the early to middle stages of maturity (Gumati and Schamel, 1988; Gumati at el., 1996). The different reservoirs were charged by vertical migration along faults during the peak of petroleum generation in the Early Tertiary (Paleocene) (Harding, 1984).

The Sirte shales are the main seal rocks for the Cretaceous reservoirs, whereas the Hagfa shales and Hun evaporites member (anhydrite and salt deposits) of the Gir Formation are seal rocks for the Tertiary reservoirs (Abugares, 1996). The traps styles are dominantly structural (about 84%), with the remaining traps being stratigraphic or a combination of both (Clifford et al., 1980).

STRATIGRAPHY OF THE AL-BAYDA PLATFORM

The general stratigraphic column of the Al-Bayda Platform consists of the Cretaceous sandstones of the Nubian and Bahi formations, overlain by Late Cretaceous–Eocene limestones, dolostones, and Paleogene shales (Sinha and Mriheel, 1996). The two studied wells (F22-59W and F24I-59W) are located on the Khalifa High of the Al-Bayda Platform, and are separated by a normal fault, with a throw of 149 m (Figure 2). The Cretaceous sandstones are found in the study wells at depths between 2,127 (-1,866) m and 2,271 (-2,015) m. The bottom-hole temperature is about 81°C.

The Cretaceous succession in the Khalifa Field includes 77–100 m of braided fluvial sandstones of the Nubian Formation onlapped by 7–15 m of tidal sandstones of the Bahi Formation. Both formations are onlapped by Late Cretaceous shallow-marine Lidam dolomite (Figure 2). The tidal Bahi sandstones occur in northwestern (Az-Zahrah-Al-Hufrah Platform), northeastern and southern (Al-Bayda Platform) parts of the basin. The Nubian sandstones are Lower Cretaceous in age according to Barr and Weegar (1972). The Nubian Formation unconformably overlies a basement consisting of quartzite in the Bahi Field and Cambrian granite in the Khalifa Field, and is unconformably overlain by various Late Cretaceous marine deposits (Barr and Weegar, 1972). The age of Bahi sandstones ranges from the Cenomanian to Maastrichtian (Barr and Weegar, 1972; Sghair, 1996).

The graphic logs description for the two wells (Figures 3a and b), reveals that the fining-upward Nubian sandstones are coarse-grained to conglomeratic, poorly sorted and trough cross-bedded. The

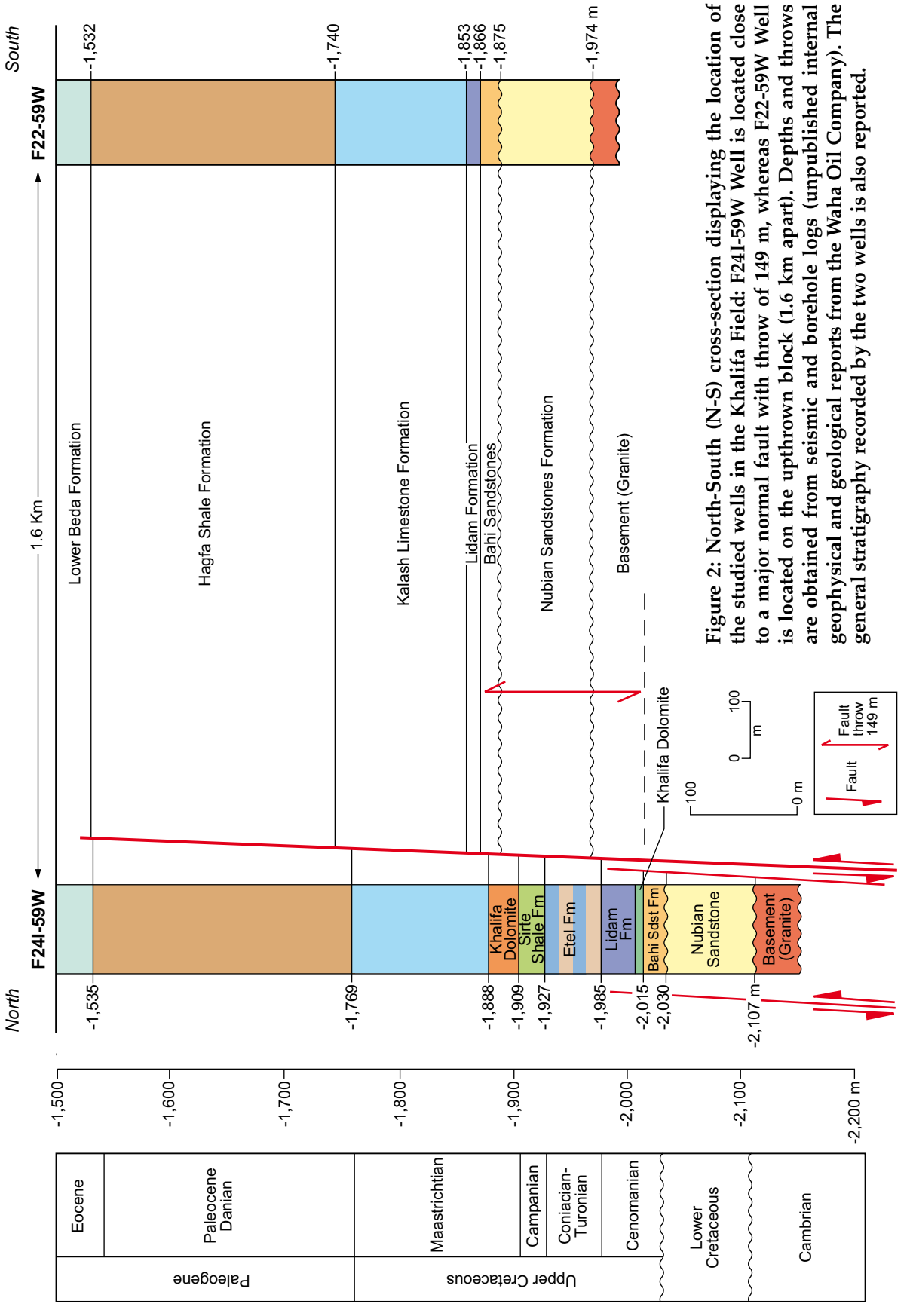

Figure 2: North-South (N-S) cross-section displaying the location of the studied wells in the Khalifa Field: F24I-59W Well is located close to a major normal fault with throw of 149 m, whereas F22-59W Well is located on the upthrown block (1.6 km apart). Depths and throws are obtained from seismic and borehole logs (unpublished internal geophysical and geological reports from the Waha Oil Company). The general stratigraphy recorded by the two wells is also reported.

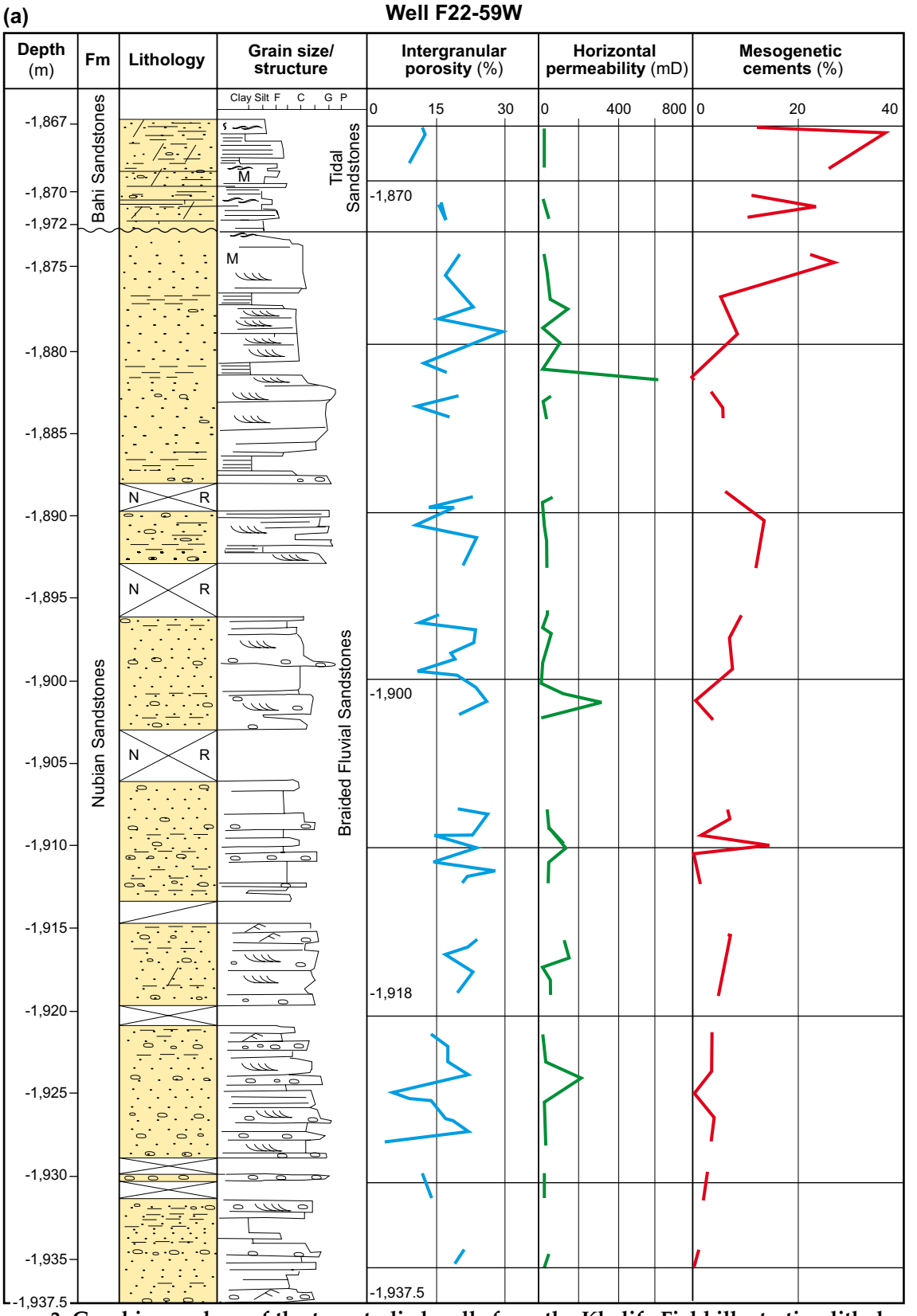

Figure 3: Graphic core logs of the two studied wells from the Khalifa Field illustrating lithology, texture, depositional environment, porosity, permeability and amount of deep-burial cements in vol% (see also Table 1). (a) Graphic core log of Well F22-59W of the upthrown block. Note that the tidal Bahi sandstones are characterized by low to moderate helium porosity, low permeability and high deep-burial (carbonate) cementation, whereas the braided fluvial Nubian sandstones are characterized by high helium porosity, low to moderate permeability and display gradual decrease in the amount of deep-burial cements (illite and silica) in the lower part of the log, likely due to previous chlorite precipitation. Kelly bushing: 261 m. Ground level: 255 m.

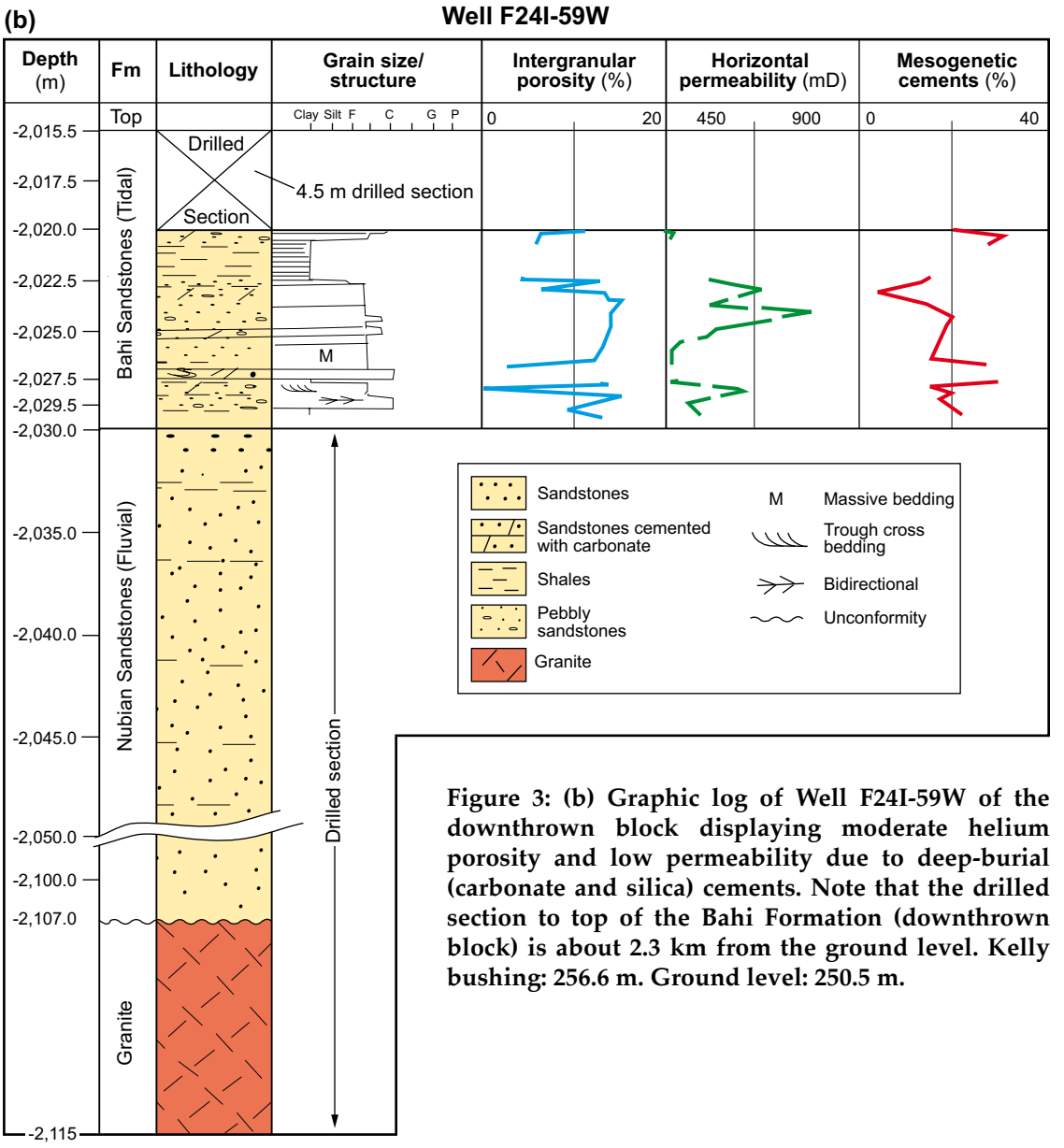

Figure 3: (b) Graphic log of Well F24I-59W of the downthrown block displaying moderate helium porosity and low permeability due to deep-burial (carbonate and silica) cements. Note that the drilled section to top of the Bahi Formation (downthrown block) is about 2.3 km from the ground level. Kelly bushing: 256.6 m. Ground level: 250.5 m.

individual sandstones cycles vary in thickness from 3 to 6 m and are marked at the base by very coarse-grained, pebbly and conglomeratic channel lags or by scoured surfaces. The sandstone cycles, which are interpreted as braided fluvial sandstones, are interbedded with planar-bedded floodplain claystones (< 1 to 3 m thick). On the other hand, the Bahi sandstones are fine-to medium-grained with planar and flaser bedding and soft-sediment deformation structures. These sandstones are interbedded with claystone beds (1–2 m thick) commonly bearing thin beds of sandstones, which are interpreted as shallow-marine tidal deposits.

SAMPLES AND ANALYTICAL METHODS

A set of 137 core samples was collected from the two studied wells (F22-59W and F24I-59W) of the Khalifa Field (Figure 1c). The subsea depths of the cored sandstone sections of both Bahi and Nubian formations range from 2,127 to 2,197 m (70 m) in the upthrown block (well F22-59W), and from 2,277 to 2,286 m (9 m) of only the Bahi Formation in the downthrown block (well F24I-59W) (Figure 2). Polished thin sections were prepared for all selected samples subsequent to vacuum impregnation with blue-colored epoxy. The modal compositions were obtained for 67 thin sections by conventional point

counting according to Harwood (1988) using 300 points per thin section, including framework grains, cement, and porosity. The 2 sigma (σ) standard deviation for each individual mineral component per thin section was calculated according to Van der Plas and Tobi (1965). Scanning Electron Microscopy (SEM) was conducted on 20 gold-coated chips from representative samples in order to study the texture, pore-scale distribution and paragenetic relationships of diagenetic alteration.

A set of 18 polished thin sections representing the different depositional facies were thinly coated with carbon in order to accomplish Electron Microprobe (EMP) analysis using a Cameca SX50 instrument, equipped with three spectrometers and a backscattered electron detector (BSE). Operating conditions during the analysis were: an accelerating voltage of 20 kV, a beam current of 10 A (for carbonates) and 15 A (for silicates) and a spot size of 1 to 5 μm. Analytical precision [(standard deviation/mean) x 100)] was < 1% for Ca, < 5% for Mg, < 25% for Mn, and < 9% for Fe.

For carbon- and oxygen-isotope analyses 9 calcite cemented samples were reacted in vacuum with 100% phosphoric acid at 25°C during one hour (Al-Aasm et al., 1990). The collected CO_2 was analyzed using a delta plus mass spectrometer. The phosphoric acid fractionation factor used was 1.01025 for calcite (Friedman and O'Neil, 1977). Oxygen and carbon stable-isotope data are reported in per mil (‰) relative to V-PDB standard (Craig, 1957).

The clay fractions < 2 μm from 3 sandstone samples were separated by decantation methods. Orientated samples were placed onto glass slides, and X-ray diffraction (XRD) analysis was performed on air dried as well as glycolated perpetrates, and heated at 350°C and 550°C for four hours.

Fluid inclusion microthermometry was conducted on 4 samples from the F24I-59W and F22-59W wells. Primary fluid inclusions in authigenic quartz from thick polished sections were analyzed on a Linkam MDS 600 heating-freezing stage, mounted on Nikon LV 100 Eclipse, which was calibrated by using synthetic fluid inclusions of known composition. Petrography according to Goldstein and Reynolds (1994) allowed distinguishing different types of fluid inclusions. A mercury vapor lamp (100 W) attached to the petrographic microscope allowed UV-light to check for the presence of aromatic hydrocarbons. The accuracy of the data is ±3°C for homogenization temperatures (Th) and ±0.2°C for the melting temperatures (Tm). Heating runs were repeated twice on many inclusions to check for leakage. The Linksys 32 software enabled all the operations for fluid inclusion petrography and microthermometry. Salinity estimation for aqueous inclusions was based on final melting temperatures of ice (Tm_i) using the equation of Bodnar (1993) for the binary NaCl-H_2O system.

Porosity and permeability were measured on core plugs 3.8 cm in diameter obtained from 108 sandstone samples. The porosity measurements were performed using helium porosimeter, whereas permeability measurements were achieved using helium permeameter by applying a confining pressure of 100 to 400 psi. Prior to measurements, the core plugs were examined carefully for microfractures, cleaned in an oil extractor, and dried in a vacuum oven at 60°C for twenty-four hours.

DETRITAL COMPOSITION OF THE SANDSTONES

The modal analyses (Table 1; Figure 4) indicate that the sandstones are dominantly subarkoses and, to a smaller extent, quartz-arenites with average composition of $Q_{83}F_{16}L_1$. The framework grains are dominated by monocrystalline quartz (26–57 vol%, average 45 vol%) and polycrystalline quartz (0.3–16.3 vol%, average 6.6 vol%). Microcline and perthite dominate over plagioclase (< 1–16 vol%, average 10 vol%). Other sands include trace amounts of mica (muscovite and rare biotite, 0–4 vol%, average 1 vol%). Rock fragments (0–2 vol%, average 1 vol%) are dominated by micrographic texture, which may suggest igneous sources and coarse polycrystalline quartz. Heavy minerals (< 1.5 vol%) include zircon, rutile and tourmaline. The framework modal compositions show that the Cretaceous sandstones from the tidal Bahi and braided fluvial Nubian formations sampled from the wells F22-59W and F24I-59W fall in the craton interior and transitional continental fields according to the model by Dickinson et al. (1983).

Table 1
Framework composition and diagenetic cement abundance within the tidal Bahi and the braided fluvial Nubian sandstones from the two studied wells: F22-59W and F24I-59W. The values represent volume in %. SD stands for standard deviation.

Rock Composition	Upthrown Block Well F22-59W										Downthrown Block F24I				
	Tidal sandstones					Braided fluvial sandstones					Tidal sandstones				
Detrital component	Min	Max	Mean	SD	2σ	Min	Max	Mean	SD	2σ	Min	Max	Mean	SD	2σ
Monocrystalline quartz	31.9	50.4	42.1	2.4	4.8	31	55.3	48.8	2.8	5.6	23	57	44.3	2.8	5.6
Polycrystalline quartz	1.6	10.3	6.4	1.1	2.2	0.3	16.3	6.8	1.4	2.8	2	10.3	5.8	1.2	2.4
Feldspar	0.3	14.3	7.6	1.2	2.4	3.3	16	9.2	1.6	3.2	5.3	16	10	1.6	3.2
Rock fragments	n.d	1.3	0.5	0.2	0.4	0.5	2	0.3	0.2	0.4	n.d	2	0.7	0.4	0.8
Mica	0.3	0.6	0.5	0.1	0.2	n.d	4	0.6	0.3	0.6	n.d	2.3	0.3	0.3	0.6
Heavy minerals	0.3	tr	n.d	n.d	n.d	n.d	1.6	1	0.1	0.2	n.d	0.6	n.d	0.1	0.2
Diagenetic component															
Quartz overgrowths	1.3	11.3	4.64	0.9	1.8	n.d	13	3.6	0.9	1.8	0.6	18	11	1.6	3.2
Dolomite and ankerite	7	41.5	21.5	2.1	4.2	n.d	22	2.5	0.5	1	n.d	16	1.6	0.7	1.4
Calcite	n.d	3	0.6	0.5	1	n.d	4	1	n.d	n.d	n.d	23	5.2	0.6	1.2
Siderite	n.d	n.d	n.d	n.d	n.d	n.d	3	0.1	n.d	n.d	n.d	7	0.5	n.d	n.d
Illite	n.d	17.9	4.8	0.5	1	1	40	17.3	1.1	2.2	n.d	27	3.5	0.6	1.2
Kaoline	n.d	2.3	0.6	0.2	0.4	n.d	3	0.5	0.2	0.4	n.d	n.d	n.d	n.d	n.d
Chert/chalcedony	n.d	1	0.3	n.d	n.d	n.d	10	n.d	n.d	n.d	n.d	1	0.1	n.d	n.d
Chlorite	n.d	n.d	n.d	n.d	n.d	n.d	1	0.1	n.d	n.d	0	5	1	n.d	n.d
Anhydrite	n.d	n.d	n.d	n.d	n.d	n.d	n.d	n.d	n.d	n.d	n.d	2	0.3	n.d	n.d
Barite	n.d	n.d	n.d	n.d	n.d	n.d	n.d	n.d	n.d	n.d	n.d	7	0.6	0.2	0.4
Porosity															
Intergranular	n.d	19.3	6.59	0.9	1.8	0.3	24	11	5.7	11.4	n.d	19	13	1.8	3.6
Intragranular	n.d	n.d	n.d	n.d	n.d	n.d	1.6	n.d	n.d	n.d	n.d	1	0.1	n.d	n.d
Moldic porosity	n.d	n.d	n.d	n.d	n.d	n.d	3.3	1.4	1.3	2.6	n.d	1	0.14	n.d	n.d

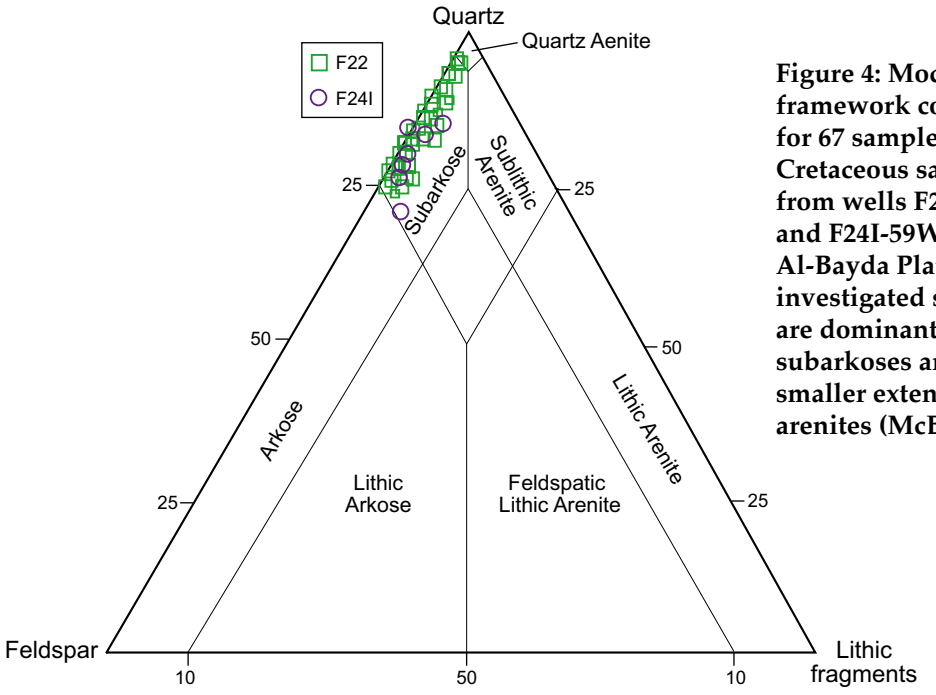

Figure 4: Modal framework composition for 67 samples of Cretaceous sandstones from wells F22-59W and F24I-59W of the Al-Bayda Platform. The investigated sandstones are dominantly subarkoses and, to a smaller extent, quartz arenites (McBride, 1963).

DIAGENETIC CONSTITUENTS

Quartz Overgrowths, Micro-quartz and Chalcedony

Quartz and chalcedony (from traces up to 16 vol%) are among the main cements in the studied sandstones. Quartz cement occurs as syntaxial overgrowths (up to 100 μm thick), which cover the detrital grains partly to completely (Figure 5a). Quartz also occurs as numerous tiny crystals (micro-quartz, < 10 μm across) and as discrete prismatic crystals (outgrowths up to 70 μm long) on quartz grains. Quartz over- and outgrowths are later than grain-coating illite (Figure 5b), kaolinite (Figure 5c) and chlorite (Figure 5d). The quartz overgrowths are coated by ferroan-dolomite, ankerite and calcite (Figure 5e) as well as anhydrite (Figure 5f). Mutual cross-cutting relationships between quartz overgrowths and barite suggest co-precipitation of these two phases (Figure 6a and b). Micro-quartz occurs as numerous tiny euhedral crystals coating detrital quartz grains, with no quartz overgrowths developed where extensive micro-quartz precipitated. The euhedral micro-quartz crystals would have coalesced locally to form larger quartz crystals (Figure 6c). Micro-quartz occurs only in the braided fluvial Nubian sandstones of the upthrown block. The quartz overgrowths are absent when the grains are extensively coated by clay minerals or by micro-quartz. Quartz overgrowths are more abundant (average 11 vol%) in the tidal Bahi sandstones of the downthrown block than in the tidal Bahi and the braided fluvial Nubian sandstones of the upthrown block (average 4 vol%). Chalcedony (up to 10 vol%) occurs in few samples of the braided fluvial Nubian sandstones, filling pore space and overgrowing grain-coating clays (Figure 6d).

Fluid inclusions in quartz overgrowths from tidal Bahi and braided fluvial Nubian sandstones, which display similar mineralogical composition and diagenetic evolution, were investigated. Various types of inclusions were distinguished according to their petrographic distribution within quartz grains and overgrowths. Fluid inclusions within detrital quartz grains were not analyzed because they formed prior to diagenesis. On the other hand, the fluid inclusions in quartz overgrowths were analyzed in order to obtain information about precipitation temperatures and water salinity. The inclusions in quartz overgrowths were distinguished in three groups according to their geometry: (1) Primary, located along the rim between the quartz grain and overgrowth (Figure 6e); (2) Pseudo-secondary controlled by growth directions and located along trails propagating from boundary between quartz grain and overgrowth; and (3) Primary isolated and not following a trail (Figure 6f).

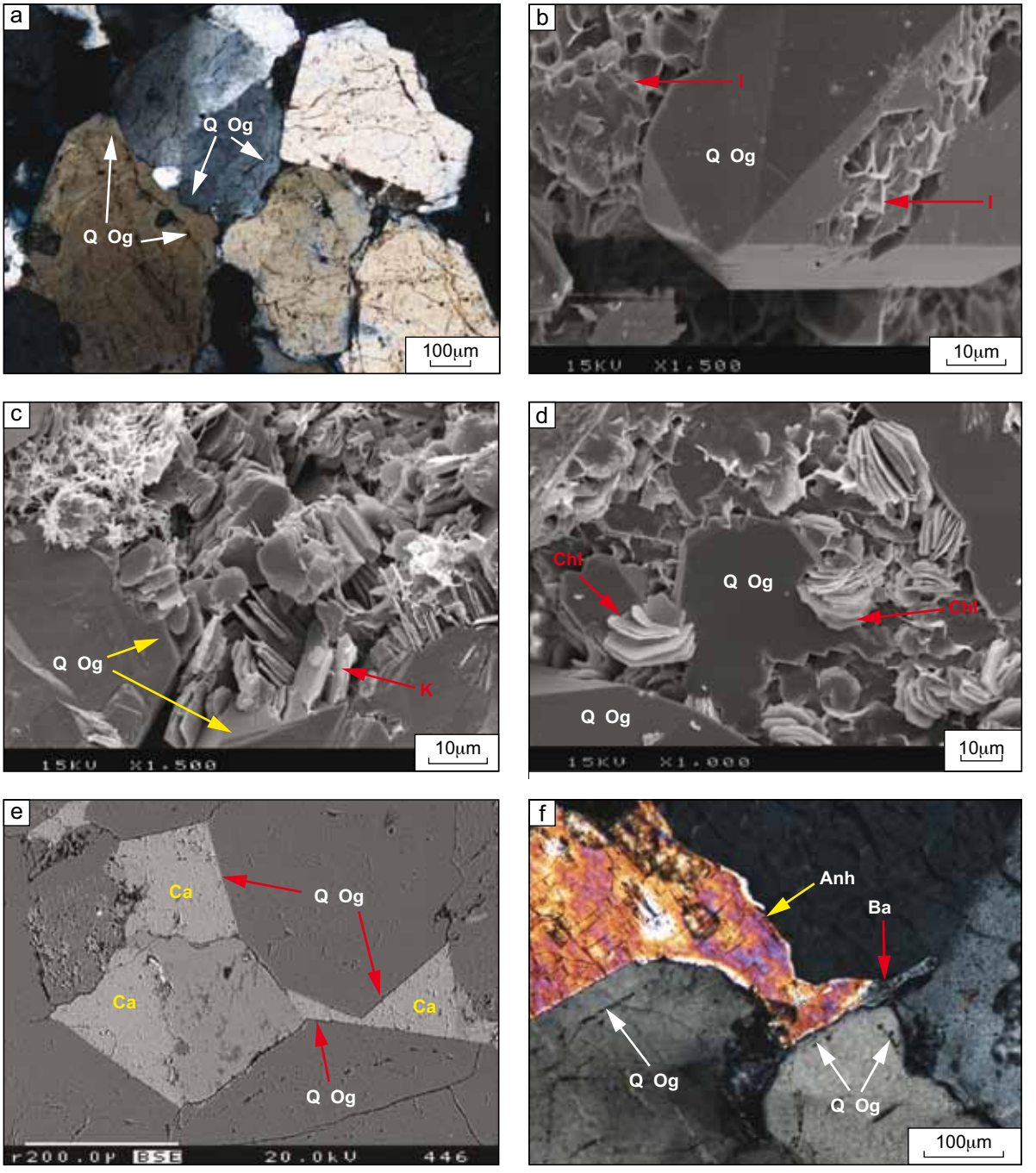

Figure 5: (a) Optical photomicrograph (XPL) showing straight and intergrowth contacts between syntaxial quartz overgrowths (arrows), which reduced the intergranular porosity. Medium-grained, tidal Bahi sandstones of downthrown block. (b) SEM image showing a quartz overgrowth (Q Og), which overgrows and thus post-dates honeycomb-like illite (I; arrows). Medium-grained, braided fluvial Nubian sandstones of upthrown block. (c) SEM image showing a quartz overgrowth (Q Og; yellow arrows) which overgrows, and thus post-dates kaolin (K; red arrow). Medium-grained, braided fluvial Nubian sandstones of upthrown block. (d) SEM image showing a quartz overgrowth (Q Og), overgrows, and thus post-dates chlorite (Chl; arrows). Medium-grained, tidal Bahi sandstones of downthrown block. (e) Back-scattered Electron (BSE) image showing quartz overgrowths (Q Og; arrows) overgrown by late calcite (Ca). Medium-grained, tidal Bahi sandstones of downthrown block. (f) Optical photomicrograph (XPL) showing a quartz overgrowth (Q Og; white arrows) post-dated by anhydrite (Anh; yellow arrow). Note that anhydrite also overgrows barite (Ba; red arrow). Medium-grained, tidal Bahi sandstones of downthrown block.

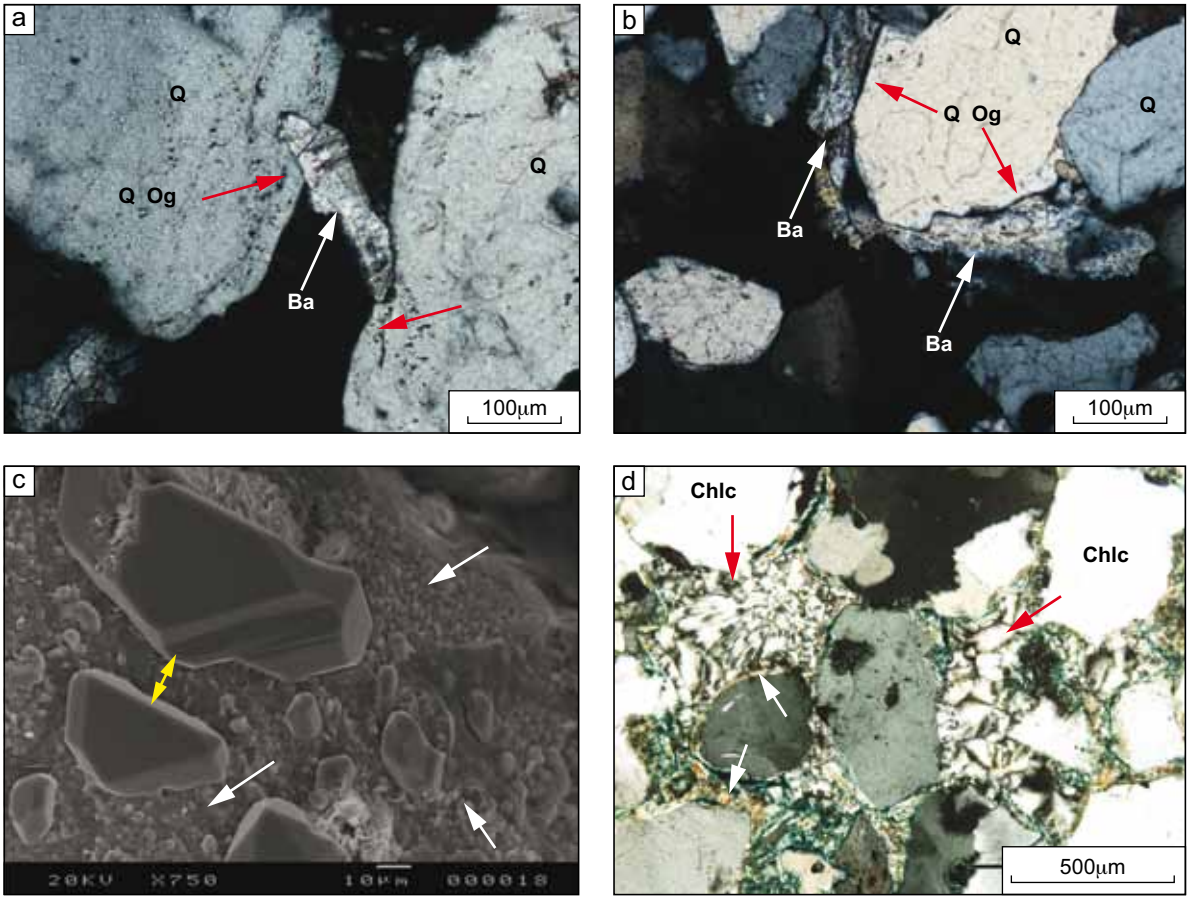

Figure 6: (a) Optical photomicrograph (XPL) showing quartz overgrowths (Q Og; red arrows) overgrows barite (Ba; white arrow). Medium-grained, tidal Bahi sandstones of downthrown block. (b) Optical photomicrograph (XPL) showing quartz overgrowth (Q Og; red arrows) overgrown by barite (Ba; white arrows). Medium-grained, tidal Bahi sandstones of downthrown block. (c) SEM image showing micro-quartz (white arrows) coating detrital quartz grains. Note that the tiny (< 10 μm) euhedral quartz crystals have coalesced locally to form larger quartz crystals (yellow arrows). Medium- to coarse-grained, braided fluvial Nubian sandstones of upthrown block. (d) Optical photomicrograph (XPL) showing chalcedony (Chlc; red arrows), which occupies pore spaces and overgrows infiltrated clay coating (white arrows). Medium-grained, braided fluvial Nubian sandstones of upthrown block.

The three types of inclusions occur dominantly as two-phase liquid-rich assemblages (Figure 6g), are mainly elongated to irregular in shape and with size ranging from < 3 μm to 15 μm. Furthermore, these inclusions display similar behavior during micro-thermometric measurements, and are considered representative of the same fluid system. The homogenization occurred in the liquid phase with normal behavior. The nucleation of the gas bubble occurred at temperatures between 70°C and 100°C. Nucleation of the ice-like phases occurs during the first cooling run at temperatures between -42°C and -59°C. The appearance of the first liquid (eutectic temperature) occurs in two different ways: sudden or by gradual melting of an unknown salt-hydrate. The sudden and gradual first melting occurs at temperatures between -20°C and -34°C, suggesting the presence of other dissolved salts beside NaCl. After the first liquid occurred, only ice remained in the fluid inclusions. The final melting of ice (Tm_f) occurred with no metastability phenomena.

High temperature microthermometry runs revealed homogenization temperatures (Th) mainly in the range between 90°C and 120°C (mode is 100–110°C), whereas low temperature runs revealed final ice melting temperatures (Tm_f) mainly in the range between -10°C to -15°C (mode is -13°C) (Figures 7a and b). The salinity of the inclusion fluids (Figure 7c) calculated according to Bodnar (1993) ranges between 15 and 19 wt% NaCl equivalent.

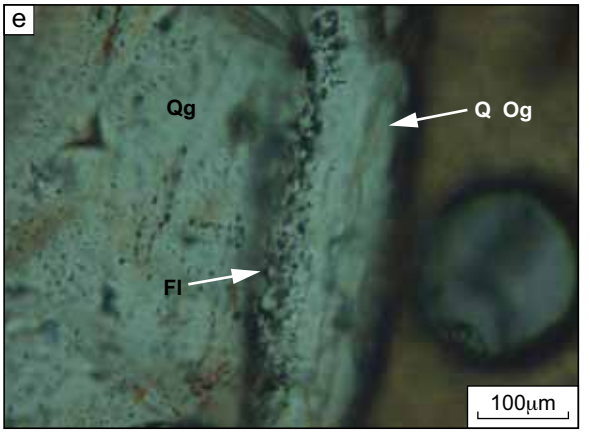

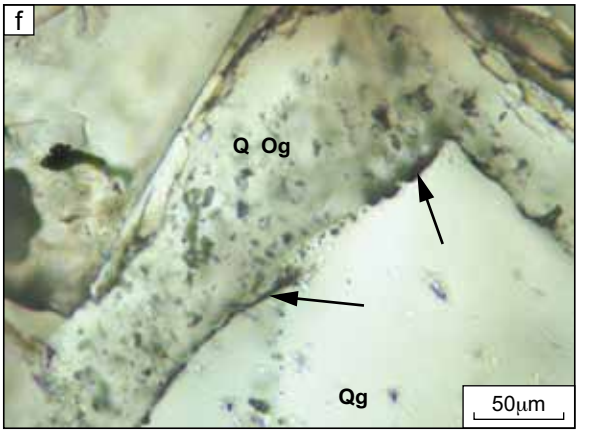

Figure 6 *continued*: (e) Optical photomicrograph (PPL) showing fluid inclusion trail (white arrow) occurring along the dust rim between quartz grain (Qg) and quartz overgrowth (Q Og; white arrow). Coarse-grained, tidal Bahi sandstones of downthrown block. (f) Optical photomicrograph (PPL) showing fluid inclusions isolated and not following trails within a quartz overgrowth (Q Og). (g) Optical photomicrograph (PPL) showing a closer view of an irregular shaped two-phase liquid-rich fluid inclusion (FI; arrow) within a quartz overgrowth.

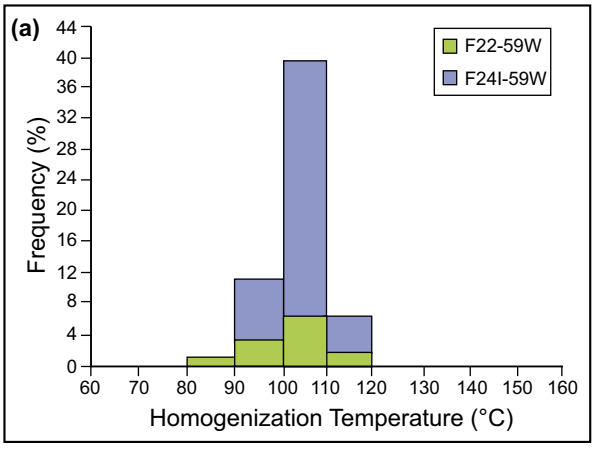

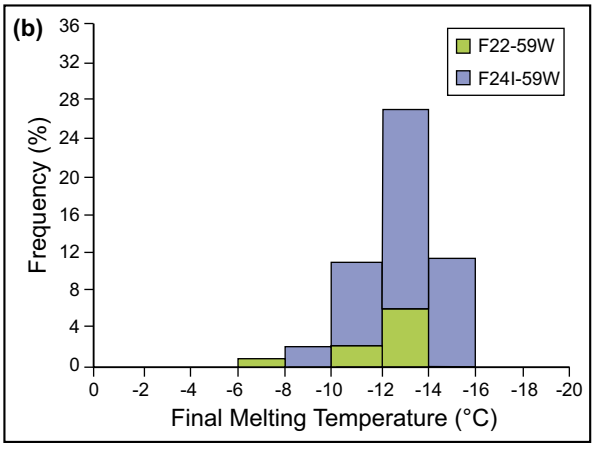

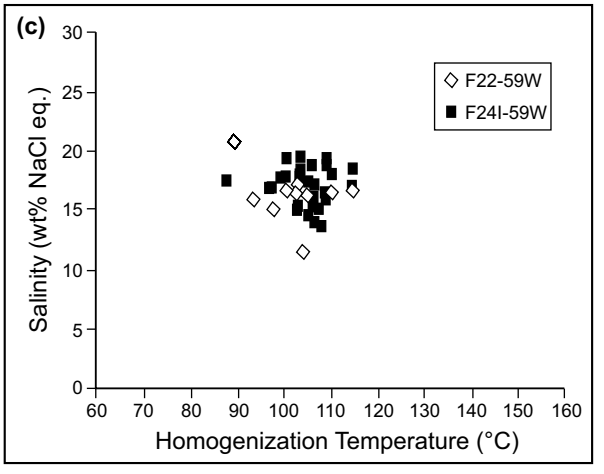

Figure 7: Main results of microthermometry on fluid inclusions from quartz overgrowths. Data represent the two studied wells F22-59W and F24I-59W. (a) Frequency distribution of homogenization temperatures (Th). (b) Frequency distribution of final melting temperature of ice (Tm_f). (c) Clustering of homogenization temperatures (Th) *versus* salinities (wt% NaCl eq.).

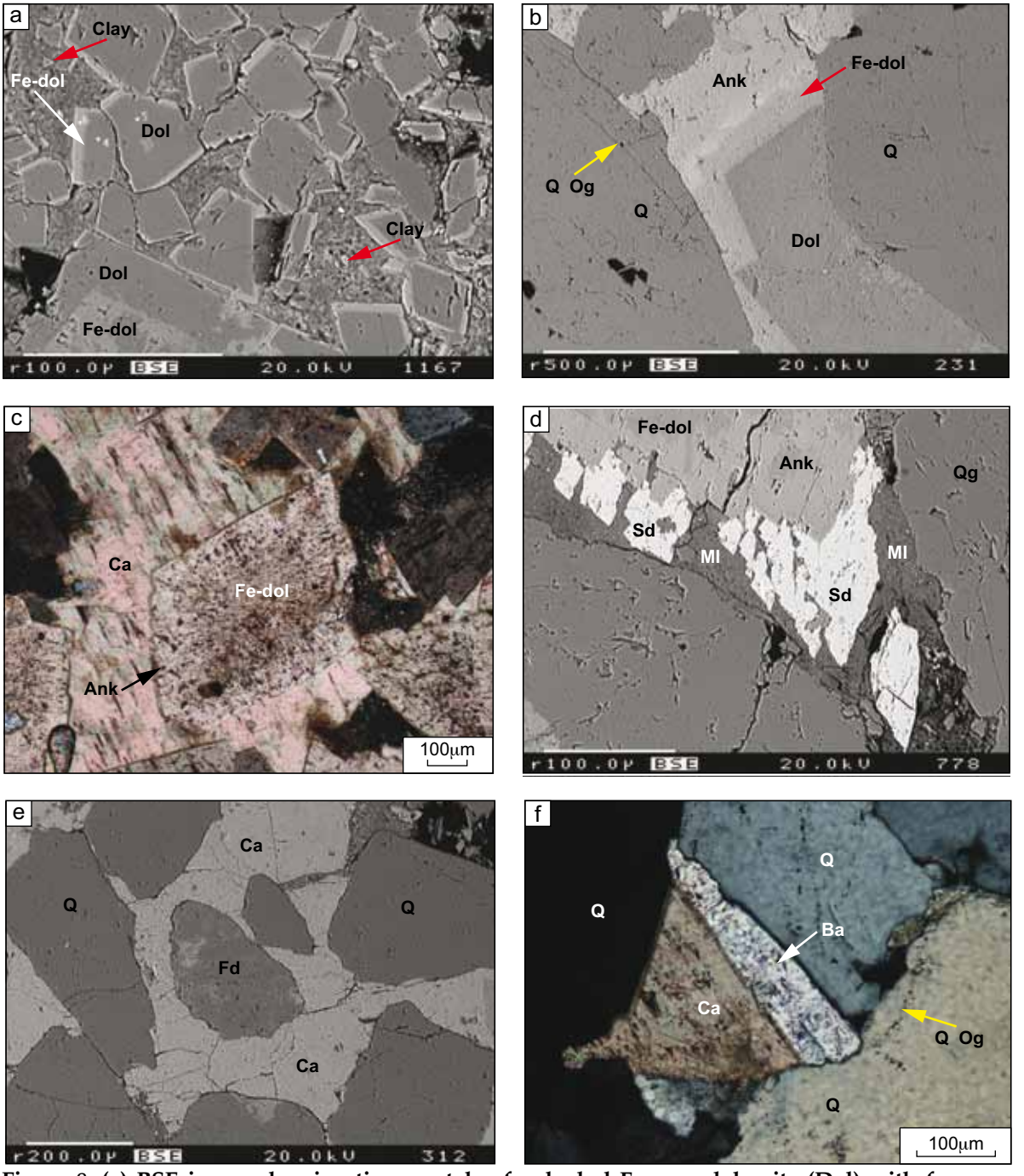

Figure 8: (a) BSE image showing tiny crystals of euhedral Fe-poor dolomite (Dol) with ferroan-dolomite overgrowth (Fe-dol; white arrow), which also replaces mud intraclast (red arrows). Note the large euhedral Fe-poor dolomite crystal with the core partially replaced by ferroan-dolomite. Dolomite cemented sandstones, the tidal Bahi sandstones of upthrown block. (b) BSE image of a coarse dolomite (Dol) and ankerite (Ank) crystal, showing gradual increase of Fe content from the core (Fe-poor dolomite) towards the most external rim (ferroan-dolomite and ankerite). Note that the Fe-poor dolomite (Dol) overgrows quartz grains, whereas the ferroan-dolomite (red arrow) and ankerite overgrows quartz overgrowths (yellow arrow). Medium-grained, tidal Bahi sandstones of downthrown block. (c) Optical photomicrograph (XPL) showing euhedral ferroan-dolomite (Fe-dol) crystal with an ankerite overgrowth (Ank; black arrow), which replaces and hence post-date poikilotopic calcite (Ca) crystals. Dolomitic sandstone beds, the tidal Bahi sandstones of downthrown block. (d) BSE image showing siderite (Sd) replacing mud intraclast (MI) and overgrowing ankerite (Ank). Coarse-grained, braided fluvial Nubian sandstones of upthrown block.

Carbonate Cements

Carbonate cements include dolomite, ankerite, calcite, and siderite. These cements are more common in the tidal Bahi sandstones (14.5 vol%) than in the braided fluvial Nubian sandstones (3.5 vol%). Fe-poor dolomite is replaced and overgrown by ferroan-dolomite and ankerite (Figures 8a and b). The ferroan-dolomite and ankerite overgrew feldspar and quartz overgrowths (Figure 8b), replace poikilotopic calcite (Figure 8c), and are in turn overgrown by siderite (Figure 8d). Microprobe analyses of Fe-poor dolomite (Figure 9; Table 2) revealed an average composition of $Ca_{57.2}Mg_{41.1}Mn_{0.4}Fe_{1.3}Sr_{0.01}CO_3$. Conversely, ferroan-dolomite and ankerite have the following average composition: $Ca_{55.4}Mg_{19.3}Mn_{0.5}Fe_{27.3}Sr_{0.01}$.

Calcite occurs as poikilotopic (up to 500 μm across) and as blocky crystals filling intergranular pores, and is more abundant (up to 23 vol%) in the tidal Bahi sandstones on the downthrown block. Poikilotopic calcite overgrows framework grains with no or little quartz or feldspar overgrowths (Figure 8e), whereas late calcite overgrows quartz overgrowths (Figure 5e) and barite (Figure 8f). Microprobe analyses of calcite cements (Table 2) revealed small amounts of Mg (0–0.9‰), Mn (0–2.2‰), Fe (0–3.2‰) and Sr (0–0.6‰). The calcite cement that did not overgrow quartz overgrowths has $\delta^{18}O_{V\text{-}PDB}$ values from -9.8‰ to -7.0‰ and $\delta^{13}C_{V\text{-}PDB}$ from -4.2‰ to -3.4‰, whereas the calcite that overgrows quartz overgrowths has $\delta^{18}O_{V\text{-}PDB}$ values from -10.0‰ to -8.8‰ and $\delta^{13}C_{V\text{-}PDB}$ from -5.7‰ to -3.8‰.

Siderite (0–7 vol%), which occurs as small crystals in the tidal Bahi and braided fluvial Nubian sandstones, has an average molar composition of $Fe_{83}Ca_{6.3}Mg_{10.2}Mn_{0.5}Sr_{0.03}$. Siderite commonly replaces the mud intraclasts and overgrows the ferroan-dolomite and ankerite (Figure 8d), as well as quartz overgrowths.

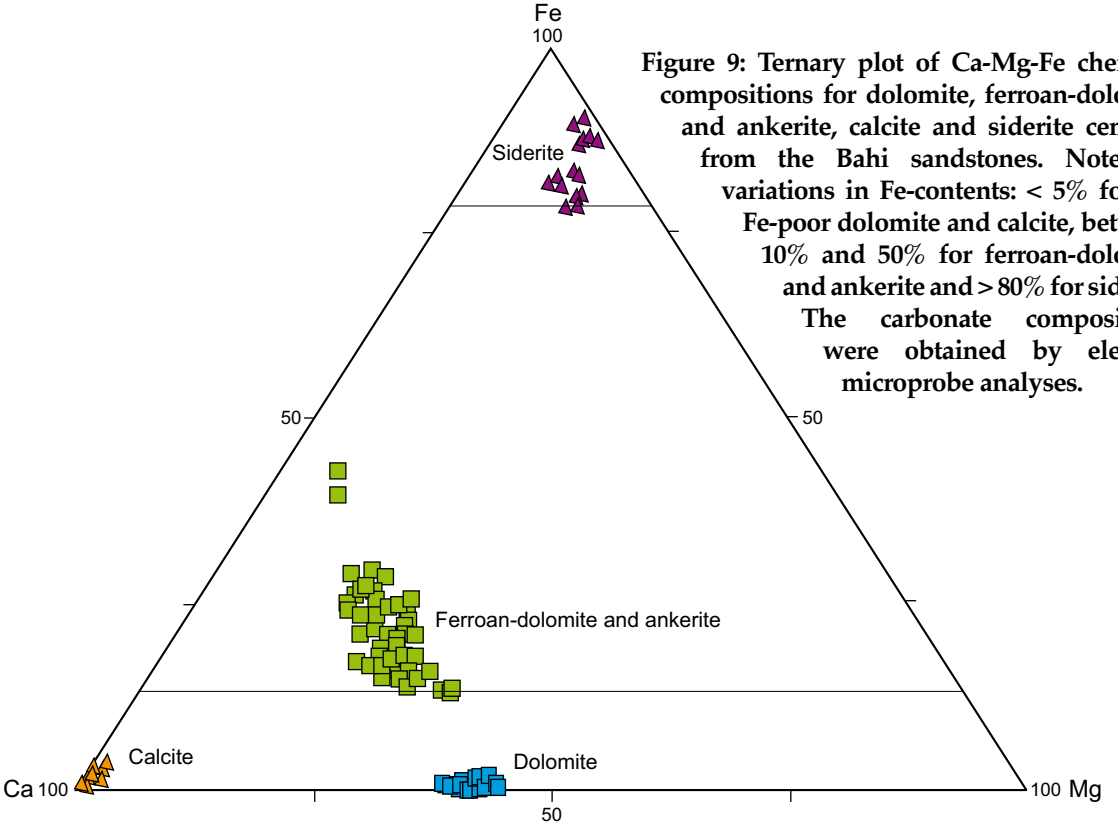

Figure 9: Ternary plot of Ca-Mg-Fe chemical compositions for dolomite, ferroan-dolomite and ankerite, calcite and siderite cements from the Bahi sandstones. Note the variations in Fe-contents: < 5% for the Fe-poor dolomite and calcite, between 10% and 50% for ferroan-dolomite and ankerite and > 80% for siderite. The carbonate compositions were obtained by electron microprobe analyses.

Figure 8 *continued*: (e) BSE image showing early blocky calcite (Ca), which overgrows framework grains (Q: quartz and Fd: feldspar) in the absence of quartz overgrowths. Medium-grained, tidal Bahi sandstones of downthrown block. (f) Late calcite (Ca) cement overgrows quartz overgrowth (Q Og; yellow arrow) and barite (Ba; white arrow), and thus post-dated. Medium-grained, tidal Bahi sandstones of downthrown block.

Table 2

Microprobe analyses (expressed in mole%) for carbonate cements together with oxygen and carbon stable-isotope analyses of calcites for samples from the tidal Bahi and the braided fluvial Nubian sandstones of the studied wells.

Well name	Depth (m)	Sample no.	Mineral	No. of analyses	$MgCO_3$ mole%	$CaCO_3$ mole%	$MnCO_3$ mole%	$FeCO_3$ mole%	$SrCO_3$ mole%	$\delta^{13}C_{V\text{-}PDB}$ (‰)	$\delta^{18}O_{V\text{-}PDB}$ (‰)
F22-59W Up-thrown block	2,124.60	9	dolomite	8	41.1	58.3	0.2	0.4	0.03		
			Fe-dolomite	4	31.4	53.9	0.6	14.2	0.01		
			ankerite	7	23.3	53.2	0.4	22.8	0.01		
	2,128.40	11	dolomite	2	38.4	59.8	0.5	1.2	0.03		
			fe-dolomite	3	20.1	54.2	0.3	25.4	0.02		
			ankerite	5	25.3	56.9	0.5	17.2	0.01		
	2,131.60	15	calcite	5	n.d.	99.3	0.3	0.3	0.04		
			Fe-dolomite	3	23.6	59.4	0.5	16.4	0.06		
	2,132.40	16	calcite	2	0.4	97.9	0.2	1.3	0.07	-3.4	-8.4
			fe-dolomite	3	23.8	56.6	0.7	19	n.d.		
			ankerite	9	19	57.8	0.3	22.8	0.08		
	2,133.60	18	calcite	13	0.2	99.7	n.d.	n.d.	0.04	-4.2	-7
	2,133.90	19	Fe-dolomite	7	23.9	58.2	0.6	17.3	n.d.		
			ankerite	10	19.7	55.7	0.3	24.3	0.02		
	2,135.50	21	dolomite	6	40.7	57.4	0.5	1.4	n.d.		
			ankerite	4	22.6	58.8	0.6	18	0.01		
	2,139.70	26	Fe-dolomite	4	24.8	56.3	0.4	18.4	0.01		
			ankerite	6	17	56	0.3	26.7	0.03		
	2,144.30	32	Fe-dolomite	1	26.4	54.5	0.5	18.6	n.d.		
			ankerite	8	18	55	0.4	26.4	0.05		
			siderite	4	9.8	8.2	n.d.	82	0.03		
F24I-59W Down-thrown block	2,274.10	1	calcite	4	0.4	98.2	1.1	1.9	0.2	-5.7	-9
			dolomite	1	42.4	55.8	0.4	1.4	0		
			ankerite	4	10.9	54.5	0.4	34.1	0		
			sidirite	1	8.0	2.1	1.9	88.0	0.00		
	2,274.40	2	calcite	6	0.8	96.2	1.3	1.7	0	-4.8	-10
			siderite	3	12.9	7.9	0.0	78.6	0.1		
	2,276.50	3	calcite	4	0.8	96.4	1.3	1.5	0.03	-3.8	-8.8
			siderite	1	10.6	1.4	0.5	87.5	0.1		
	2,280.20	15	calcite	1	0.2	98.8	0.6	0.3	0.16		
	2,280.50	16	calcite	3	1.0	96.9	1.8	0.4	0.0	-6.4	-5.1
			dolomite	4	42.1	55.7	0.4	1.8	0.0		
	2,281.30	17	calcite	14	1.0	96.0	1.4	1.6	0.0		
	2,281.40	18	calcite	6	1.0	96.1	1.1	1.8	0.0	-4.2	-9.6
			siderite	4	9.3	2.8	1.3	86.6	0.0		
	2,282.60	23	calcite	4	1.1	95.6	1.2	2.1	0.0	-4.9	-9.7

Clay Minerals

Diagenetic clay minerals in the sandstones include illite, kaolin and chlorite. In the channel braided fluvial sandstones of the Nubian Formation, illite occurs (0.4–38 vol%, average 17 vol%) as grain coats (Figure 10a), as mat-like crystals arranged parallel to grain surfaces (Figure 10b) and as lath-like crystals. Illite is overgrown by quartz over- and outgrowths (Figure 5b). XRD analyses indicate the presence of mixed-layers illite/smectite (11.6 Å, 12.31 Å and 12.45 Å), which expanded after being saturated by ethylene glycol, and display a decrease in d-spacing to 10 Å when heated to 550°C according to Starkey et al. (1984) and Hillier (2003). Grain-coating illite displays shrinkage pattern, in which the coatings are detached from the grain surface (Figure 10c).

Kaolinite occurs in small amounts (0–3 vol%; Table 1) in the tidal Bahi and fluvial Nubian sandstones as scattered patches (up to 80 μm across), composed of booklet-like and vermicular stacked crystals. The thinner crystals (< 1 μm) are given by kaolinite, whereas the thicker (up to 3 μm), blocky euhedral crystals likely consist of dickite (Figure 10d). Kaolinite is overgrown by illite and quartz overgrowths (Figure 5c).

Chlorite commonly occurs as pore-filling aggregates of pseudohexagonal plates of rosette-like crystals (10–50 μm) (Figure 10e) and less commonly as pore-lining phase (Figure 10f). Chlorite is relatively abundant (0–5%) in the tidal Bahi sandstones on the downthrown block, and to a lesser extent (< 2%) in the lower part of the fluvial deposits of the Nubian sandstones on the upthrown block, but absent from the tidal Bahi sandstones on the upthrown block. Chlorite is overgrown by quartz overgrowths, and thus pre-dates quartz. Chlorite also grew with illite (i.e. honeycomb-like illite).

Sulfates

Barite occurs as euhedral tabular crystals (up to 500 μm long), which fill pore space and replace the mud intraclasts. Barite is present in small amounts (< 7 vol%) in the tidal Bahi sandstones of the downthrown block. Barite overgrows and is overgrown by quartz overgrowths (Figures 6a and 6b, respectively) and overgrows feldspar overgrowths. Anhydrite occurs in small amounts in the tidal Bahi sandstones of the downthrown block as pore-filling poikilotopic crystals (up to 350 μm across), which overgrow the quartz and feldspar overgrowths and replace the framework grains (Figure 5f).

Porosity and Permeability

Porosity of the sandstones is mainly intergranular and less commonly moldic and intragranular. Moldic porosity resulted from partial to complete dissolution of feldspar (Figure 10g), mica and mud intraclasts. Micro-porosity (< 5 μm) occurs between kaolin, illite and chlorite crystals. Intergranular porosity (0–19 vol%; average 13 vol%) occurs in the tidal Bahi sandstones of the downthrown block, as well as in the tidal Bahi sandstones of the upthrown block (average 7 vol%), moldic and intragranular porosities occur in minor amounts (≤ 1 vol%). Intergranular porosity (0.3–24 vol%, average 11 vol%), moldic porosity (0.3–3 vol %, average 1 vol%) and intragranular porosity (≤ 1.5 vol%) also occur in the braided fluvial Nubian sandstones of the upthrown block.

Core plug porosity and permeability show significant variations between the tidal Bahi and the braided fluvial Nubian sandstones. The braided fluvial sandstones have higher porosity (0–30%; average 20%) than the tidal sandstones (1.6–20%; average 11%) in both up- and downthrown blocks. The braided fluvial Nubian sandstones also display the highest horizontal permeability (< 1–6,360 mD; average 455 mD) compared to the tidal Bahi sandstones of the upthrown block (0.3–327 mD; average 106 mD) and the downthrown block (< 1–837 mD; average 168 mD). The tidal Bahi sandstones of the downthrown block have higher vertical permeability (0–792 mD; average 277 mD) than the braided fluvial Nubian sandstones (0–2,630 mD; average 163 mD) and the tidal Bahi sandstones (0–135 mD; average 23 mD) of the upthrown block.

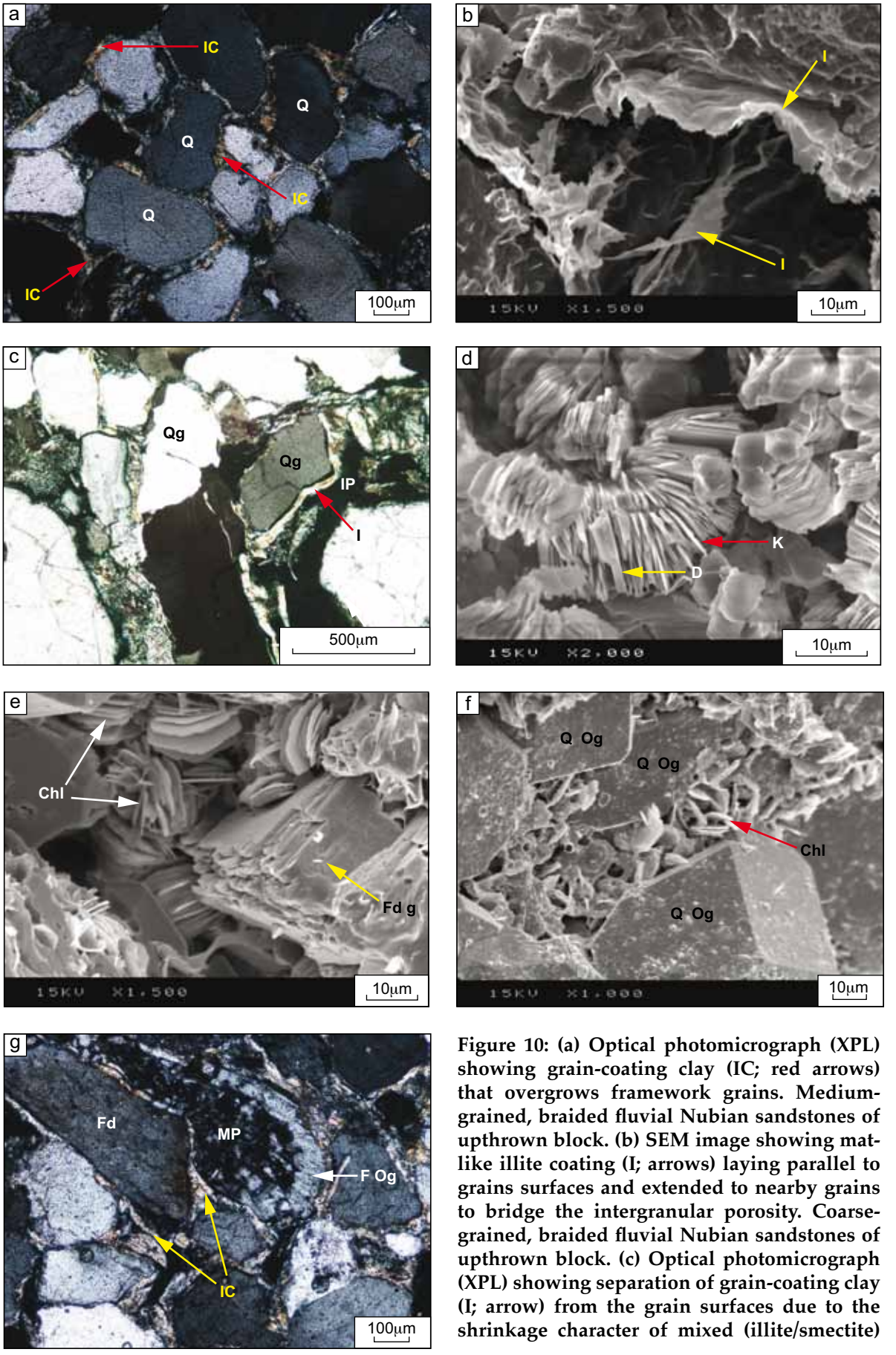

Figure 10: (a) Optical photomicrograph (XPL) showing grain-coating clay (IC; red arrows) that overgrows framework grains. Medium-grained, braided fluvial Nubian sandstones of upthrown block. (b) SEM image showing mat-like illite coating (I; arrows) laying parallel to grains surfaces and extended to nearby grains to bridge the intergranular porosity. Coarse-grained, braided fluvial Nubian sandstones of upthrown block. (c) Optical photomicrograph (XPL) showing separation of grain-coating clay (I; arrow) from the grain surfaces due to the shrinkage character of mixed (illite/smectite)

DISCUSSION

The integration of petrographic, geochemical and fluid inclusion analysis allowed reconstructing the relative timing of the main diagenetic minerals within the Nubian and Bahi sandstones on the studied upthrown and downthrown blocks (Figure 11). It is clear that significant eo- and mesodiagenesis occurred in these sandstones, which, while not completely occluding porosity, had a strong impact on reservoir quality.

The late (mesogenetic) cements are dominated by quartz overgrowths, illite, ferroan-dolomite and ankerite, siderite and to a smaller extent by anhydrite, barite and chlorite (Table 1). The distributions of these cements are controlled by variation in the distribution of early (eogenetic) calcite and grain-coating smectite, which are both dependent on the depositional facies. The abundance of quartz overgrowths and siderite, and the local occurrence of barite and anhydrite suggest the influx of hot basinal brines along faults.

According to Worden and Morad (2003), chlorite cements are deep-burial in origin (depths ≥ 3 km; temperature ≥ 90°C), and are typically formed by the transformation of precursor clays, or by direct precipitation from pore-waters (cf. Aagaard et al., 2000; Worden and Morad, 2003). Chlorite in the studied samples pre-dates quartz overgrowths with homogenization temperature of 100–110°C). However, in part chlorite was precipitated simultaneously with illite, which suggests a mesogenetic origin. The relatively abundant pore-filling chlorite consists of well-developed pseudohexagonal plates which suggest formation by direct precipitation from hydrothermal brines (Gaupp et al., 1993; Aagaard et al., 2000; Worden and Morad, 2003). Moreover, the abundant chlorite in the tidal sandstones of the downthrown block compared to the upthrown block, and chlorite occurrence in the lower part of the Nubian sandstones suggests influx of hot basinal brines (Fisher et al., 2003; Küpeli et al., 2007). The Fe and Mg ions needed for chlorite to precipitate in the Nubian sandstones of the upthrown block were possibly internally sourced from the dissolution of Fe-oxide pigments attached to the infiltrated clays (e.g. Dixon et al., 1989). Conversely, for the tidal sandstones of the downthrown block, ions needed for chlorite may have been precipitated from hot brines (e.g. Worden and Morad, 2003).

The pore-filling chlorite occludes sandstone porosity, whereas pore-lining chlorite contributed to preserve the porosity by inhibiting extensive precipitation of quartz overgrowths (e.g. Ehrenberg, 1993; Morad et al. 2010). The grain-coating illite possibly contributed to preserving porosity in the Nubian sandstones by inhibiting precipitation of quartz overgrowths in the upthrown block (e.g. Pittman et al., 1992). Here, K ions needed for illitization of clays are attributed to the dissolution of K-feldspar (e.g. Hower et al., 1976; Ehrenberg, 1991; Morad et al., 2000).

There are similarities between the late alteration of the studied sandstones and the Permian Rotliegende gas reservoirs in northwest Germany (e.g. Gaupp et al., 1993). Both reservoirs display evidence of: (1) late cementation by quartz, anhydrite and barite from the influx of hot basinal brines; and

---

Figure 10 ***continued*****:**
clay layers. Note that Qg and IP stand for quartz grains and intergranular porosity, respectively. Fine-grained, braided fluvial Nubian sandstones of upthrown block. (d) SEM image showing vermicular kaolinite (K; red arrow) and possible dickite (D; yellow arrow) filling intergranular pores. Coarse-grained, braided fluvial Nubian sandstones of upthrown block. (e) SEM image showing pore-filling chlorite (Chl; white arrows) partly occupied the intergranular porosity. Note feldspar grain (Fd g; yellow arrow). Medium-grained, tidal Bahi sandstones of the downthrown block. (f) SEM image showing grain-coating chlorite (Chl; red arrow) which overgrows quartz grains and possibly inhibited the development of syntaxial quartz overgrowths (Q Og). Coarse-grained, braided fluvial Nubian sandstones of upthrown block. (g) Optical photomicrograph (XPL) showing moldic porosity (MP), which resulted from complete feldspar grain dissolution, whereas feldspar overgrowth rims (FOg) remained unaffected. Note that grain coating illite (IC; yellow arrows) overgrows framework grains. Coarse-grained, braided fluvial Nubian sandstones of upthrown block.

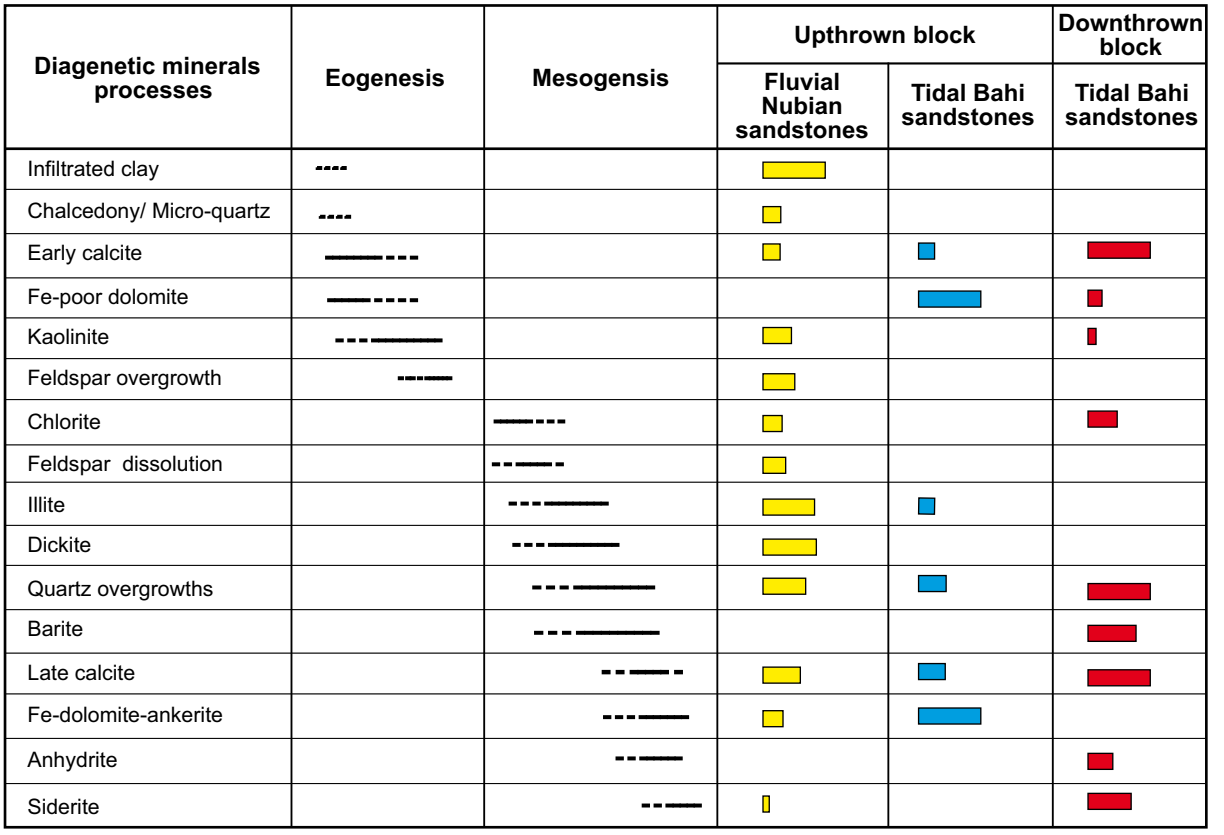

Figure 11: Paragenetic sequence suggesting the relative time relationship between the different diagenetic phases encountered in the sandstones of the tidal Bahi and the braided fluvial Nubian formations. The broad boundary between eo- and mesogenesis is assumed to be around ±70°C (according to Morad et al., 2000). Note the variations in distribution of the early and the late (eo- and mesogenetic) cements within the different depositional facies and structural settings: yellow and blue rectangles represent, respectively, the sandstones of the braided fluvial Nubian and tidal Bahi formations of the upthrown block, whereas red rectangles represent the tidal Bahi sandstones of the downthrown block. The size of the rectangles is proportional to the cement abundance.

(2) porosity preservation by grain-coating chlorite, which inhibited extensive cementation by quartz overgrowths. The main difference between the two reservoirs is the intensive dissolution of feldspar, anhydrite and carbonate cements in the Rotliegende, which was not observed in our samples.

Abundant grain-coating illite in the fluvial Nubian sandstones has possibly inhibited quartz overgrowths precipitation as compared to the tidal Bahi sandstones; the latter display no or less abundant grain-coating illite, and consequently are characterized by abundant quartz overgrowths. Similar observations are reported by Al-Ramadan et al. (2012). Moreover, the occurrence of micro-quartz in the fluvial Nubian sandstones of the upthrown block inhibited quartz overgrowths precipitation, and hence preserved porosity. Thus, micro-quartz coatings played the same role as chlorite and illite coatings in inhibiting quartz overgrowths (e.g. French et al., 2012; Worden et al., 2012).

In closed systems, Si ions needed for precipitation of quartz overgrowths are derived primarily by pressure dissolution of quartz (e.g. Oelkers et al., 1996; Fisher et al., 2003), illitization of smectite (e.g. Boles and Franks, 1979), and dissolution of feldspar grains (e.g. Morad et al., 2000). The close association of quartz overgrowths with barite, anhydrite and siderite in the Bahi sandstones of the downthrown rather than the upthrown block suggest an external source for Si, Ba and Fe ions. Hence, fluxes of hot brines via fault conduits represent the most probable source of Ba ions (cf. Haszeldine et al., 1984; Burley, 1993; Gaupp et al., 1993; Giles et al., 2000; Fisher et al., 2003; Küpeli et al., 2007). Dissolution of evaporatic

sequences in the deep subsurface normally produces sulfate-rich brines (cf. Hanor, 1994), mixing of barium-rich and sulfate-rich brines led to precipitation of barite (e.g. Gluyas et al., 1997), whereas Ca and SO_4 ions needed for precipitation of anhydrite have probably been derived from dissolution of anhydrite successions above (i.e. Etel Formation; Figure 2) (e.g. Dworkin and Land, 1994; Morad et al., 1994; Sullivan et al., 1994; Wender et al., 1998; Rossi et al., 2002; Al-Ramadan et al., 2012).

This interpretation implies that mesogenesis has occurred in open systems in which Si, Ba and Fe ions were brought by waters from deeper basinal depths, while Ca and SO_4 ions where probably brought by waters from above depths, similar results reported by Worden and Morad (2000) and Al-Ramadan et al. (2012) respectively. The flux of hot saline basinal waters probably occurred along the normal faults that bound the Al-Bayda Platform.

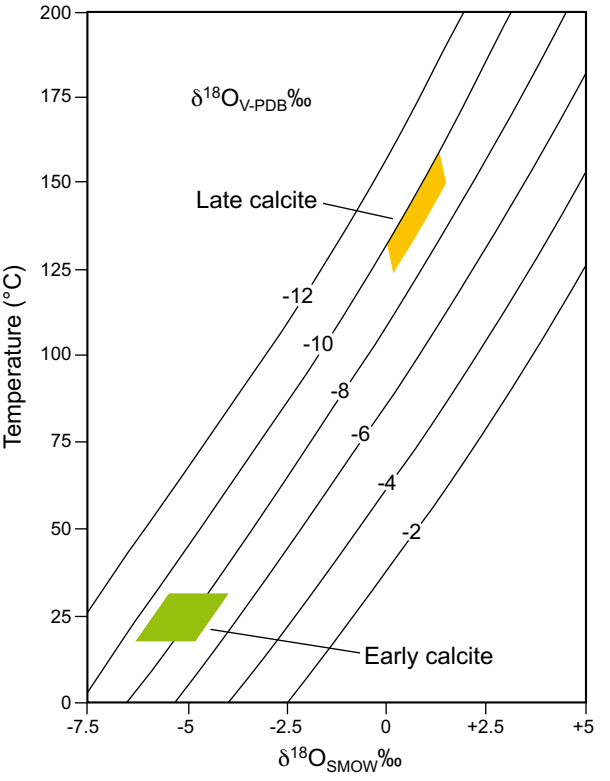

Figure 12: Range of temperature and oxygen-isotope composition of the water that precipitated the late calcite cements (orange) with $\delta^{18}O_{V\text{-}PDB}$ between -10‰ and -8.8‰, assuming a precipitation temperature between 125–160°C and using the fractionation equation of Friedman and O'Neil (1977), precipitated from waters with $\delta^{18}O_{SMOW}$ values range between 0‰ to +2‰.

The fluid inclusion homogenization temperatures (100–110°C) and salinities (16–17 wt% NaCl eq.) in quartz overgrowths are higher than present-day pore-water temperature (81°C) and salinity (10.7 wt% NaCl eq.). These temperatures may be explained as follows: (1) assuming a normal geothermal gradient of 25°C/km (Ceriani et al., 2002), the quartz overgrowths may have precipitated at greater burial depths (ca. 4.3 km) then uplifted to their current depth of ca. 2.2 km; or (2) the sandstones were subjected locally to higher temperatures. However, there is no geologic evidence in the Sirt Basin to indicate a history of deeper burial, followed by uplift and exhumation in excess of 2 km. In order to verify the second hypothesis, the quartz overgrowth homogenization temperature of 110°C was corrected to a trapping temperature of 125°C to account for hydrostatic pressure at the current depth 2.27 km using measured salinity of 17 wt% NaCl eq., and a hydrostatic pressure gradient of 10 MPa/km (Goldstein and Reynolds, 1994). Using these corrected temperatures (125°C), and assuming surface temperature of 15°C, the geothermal gradient at the time of quartz overgrowth precipitation is estimated to be about 48°C/km. This estimate is high, similar to syn-rift fluxes of hot basinal brines (50°C/km; Ceriani et al., 2002) and supports a hydrothermal origin from ascent of hot basinal brines along faults.

The late origin of some of the calcite cements is highlighted by the petrographic relationships with quartz overgrowths and barite (Figure 8f). The close association of this calcite with quartz overgrowths, barite, anhydrite and siderite in the tidal Bahi sandstones of the downthrown block suggests precipitation from hot basinal brines. Conversely, the absence of mesogenetic calcite in the upthrown block suggests that this block was less influenced by the flux of the hot basinal brines.

The oxygen isotopic composition of early diagenetic calcite ($\delta^{18}O_{V\text{-}PDB}$ = -9.8‰ to -7.0‰), assuming that it was precipitated at surface temperatures (20–30°C), and using the fractionation equation of Friedman and O'Neil (1977), indicated $\delta^{18}O_{SMOW}$ values between -6.3‰ and -4‰, which indicates precipitation from meteoric waters. The late diagenetic calcite ($\delta^{18}O_{V\text{-}PDB}$ = -10.0‰ to -8.8‰) is assumed

to have precipitated at temperature ≥ 125°C (125–160°C), the $\delta^{18}O_{SMOW}$ values will range between 0‰ and +2‰ (Figure 12), this suggests that the late calcite was precipitated from hot brines.

The high Mg content in siderite is a further indication of precipitation at higher temperatures (e.g. Morad et al., 1994; Morad, 1998). The greater abundance of siderite in the tidal Bahi sandstones in the downthrown block relative to the upthrown block suggests contribution of Mg and Fe ions from hot basinal brines (e.g. Rossi et al., 2001; Küpeli et al., 2007; Wendte et al., 2009). The oxygen isotopic composition of siderite in the northwestern part of the Sirt basin indicated precipitation at temperatures of 155–200°C (Khalifa and Morad, 2012).

The influx of hot brines along faults will inevitably lead to their cooling upon mixing with cooler connate waters in the reservoir, which is what probably caused the precipitation of deep-burial cements such as barite, anhydrite, chlorite, ferroan-dolomite, ankerite and illite (e.g. Robinson, 1992; Worden and Morad, 2000).

CONCLUSIONS

- A detailed diagenetic study of the Nubian and Bahi sandstones in the Khalifa Field of the Al-Bayda Platform (Sirt Basin, Libya) was undertaken on cores from two wells, separated by a deep-seated fault. Burial diagenesis in the upthrown block includes illitization of grain-coating smectite, precipitation of chlorite and quartz overgrowths in the braided fluvial Nubian sandstones, and to the precipitation of ferroan-dolomite and ankerite in the tidal Bahi sandstones. In the downthrown block, late alteration includes precipitation of quartz, barite, ferroan-dolomite and ankerite, anhydrite, calcite, siderite and chlorite cements in the tidal Bahi sandstones.

- The coating of detrital grains by illite, chlorite and micro-quartz have preserved porosity by inhibiting the precipitation of quartz overgrowths, whereas precipitation of abundant quartz, carbonate and barite cements have deteriorated the sandstone porosity and permeability.

- The influx of hot basinal brines into the sandstones of the downthrown block is indicated by (1) the 100–110°C homogenization temperatures of brine inclusions in quartz overgrowths, with applying pressure correction, indicate trapping temperatures between 110°C to 125°C; (2) the presence of deep-burial (mesogenetic) minerals such as barite and manganoan siderite whose component elements cannot be locally derived. Hot basinal brines are thought to have ascended along faults and permeated sandstones in the downthrown block.

- This study has demonstrated that mesogenesis of sandstones does not always occur in closed systems, but may instead involve mass fluxes of hot basinal brines in open systems that were probably fault controlled.

ACKNOWLEDGEMENTS

Muftah Khalifa would like to thank Ibrahim Al-Bagar (the General Manager of the Libyan Petroleum Institute) and Bashar Rais (the Manager of the engineering department) for their encouragement and financial support of the part-time PhD study. Many thanks go to the Libyan Petroleum Institute engineering and exploration staff for the laboratory work. Deep thanks go to Abu-Rema Abu-Algasim (the Ex-General Manager of the Libyan Petroleum Institute) for planning the PhD part-time study program. Thanks also go to the geological staff of the Waha Oil Company for providing core samples and well log data of the study area. Muftah thanks Sadoon Morad for his supervision, scientific contribution and critical reading of the manuscript and Ali Sabta for his contribution as internal supervisor. Several valuable comments and suggestions by the three reviewers of GeoArabia have helped to improve the manuscript significantly. Editor-in-Charge, Abdulkader M. Afifi, is thanked for managing the review process and Kathy Breining is thanked for proofreading the manuscript. GeoArabia's Assistant Editor, Heather Paul-Pattison, is thanked for designing the paper for press.

REFERENCES

Aagaard, P., J.S. Jahren, A.O. Harstad, O. Nilsen and M. Ramm 2000. Formation of grain-coating-chlorite in sandstones: Laboratory synthesized vs. natural occurrence. Clay Minerals, v. 35, p. 261-269.

Abugares, Y.I. 1996. Sedimentology and hydrocarbon potential of the Gir Formation, Sirt Basin. In M.J. Salem, A.S. El-Hawat and A.M. Sbeta (Eds.), The Geology of Sirt Basin. Elsevier, Amsterdam, v. 2, p. 45-64.

Ahlbrandt, T.S. 2001. The Sirt Basin province of Libya-Sirt-Zelten total petroleum system. United States Geological Survey Bulletin, 2202-F, p. 1-29.

Al-Aasm, I.S., B.E. Taylor and B. South 1990. Stable isotope analysis of multiple carbonate samples using selective acid extraction. Chemical Geology, v. 80, p. 119-125.

Al-Ramadan, K., S. Morad and P. Plink-Björklund 2012. Distribution of diagenetic alterations in relationship to depositional facies and sequence stratigraphy of a wave and tide-dominated siliciclastic shoreline complex: Upper Cretaceous Chimney Rock Sandstones, Wyoming and Utah, USA. In S. Morad, J.M. Ketzer and L.F. de Ros (Eds.), Linking Diagenesis to Sequence Stratigraphy. International Association of Sedimentologists Special Publication no. 45, p. 271-296.

Ambrose, G. 2000. The geology and hydrocarbon habitat of the Sarir Sandstone, SE Sirt Basin, Libya. Journal of Petroleum Geology, v. 23, p. 165-192.

Anketell, J.M. 1996. Structural history of the Sirt Basin and its relationships to the Sabratah Basin and Cyrenaican Platform, Northern Libya. In M.J. Salem, M.T. Busrewil, A.A. Misallati and M.A. Sola (Eds.), The Geology of Sirt Basin. Elsevier, Amsterdam, v. 3, p. 57-87.

Barr, F.T. and A.A. Weegar 1972. Stratigraphic Nomenclature of the Sirte Basin, Libya. Petroleum Exploration Society of Libya, Tripoli, 179 p.

Berger, D.G., J.C. Lacharpagne, B. Velde, D. Beaufort and B. Lanson 1997. Kinetic constraints on illitization reactions and the effects of organic diagenesis in sandstones/shale sequences. Applied Geochemistry, v. 12, p. 23-35.

Berner, R.A. 1980. Early diagenesis: A Theoretical Approach. Princeton Series in Geochemistry, Princeton University Press, Princeton, N.J., 241 p.

Bjørkum, P.A. and N. Gjelsvik 1988. An Isochemical Model for formation of authigenic kaolinite, K-feldspar and illite in sediments. Journal of Sedimentary Petrology, v. 58, p. 506-511.

Bjørkum, P.A., R. Mjøs, O. Walderhaug and A. Hurst 1990. The role of the Late Cimmerian unconformity for the distribution of kaolinite in the Gullfaks Field, northern North Sea. Sedimentology, v. 37, p. 395-406.

Bjørlykke, K. 1998. Clay mineral diagenesis in sedimentary basins-a key to the prediction of rock properties: Examples from the North Sea Basin. Clay Minerals, v. 33, p. 15-34.

Bodnar, R.J. 1993. Revised equation and table for determining the freezing point depression of H_2O-NaCl solutions. Geochimica et Cosmochimica Acta, v. 57, p. 683-684.

Boles, J.R. and S.G. Franks 1979. Clay diagenesis in Wilcox sandstones of southwest Texas: Implications of smectite diagenesis on sandstone cementation. Journal of Sedimentary Petrology, v. 49, no. 1, p. 55-70.

Burley, S.D. 1993. Models of burial diagenesis for deep exploration plays in Jurassic fault traps of the Central and Northern Sea. In J.R. Parker (Ed.), Petroleum Geology of Northwest Europe. Proceedings of the 4th Conference, London, The Geological Society of London, p. 1353-1375.

Burley, S.D., J. Mullis and A. Matter 1989. Timing of diagenesis in the Tartan reservoir UK, North Sea; Constraints from combined cathodoluminiscence microscopy and fluid inclusion studies. Marine and Petroleum Geology, v. 6, p. 98-120.

Ceriani, A., A. Di Giulio, R.H. Goldstein and C. Rossi 2002. Diagenesis associated with cooling during burial: An example from Lower Cretaceous reservoir sandstones (Sirt Basin, Libya). American Association of Petroleum Geologists Bulletin, v. 86, p. 1573-1591.

Choquette, P.W. and L.C. Pray 1970. Geologic nomenclature and classification of porosity in sedimentary carbonates. American Association of Petroleum Geologists Bulletin, v. 54, no. 2, p. 207-250.

Clifford, H.J., R. Grund and H. Musrati 1980. Geology of a stratigraphic giant, Messla oilfield, Libya. In M.T. Halbouty (Ed.), Giant Oil and Gas Fields of the Decade-1968-1978. American Association of Petroleum Geologists Memoir 30, p. 507-524.

Craig, H. 1957. The Geochemistry of stable carbon isotopes. Geochimica et Cosmochimica Acta, v. 3, p. 53-92.

De Ros, L.F., S. Morad and P.S.G. Paim 1994. The role of detrital composition and climate on the diagenetic evolution of continental molasses: Evidence from the Cambro-Ordovician Guaritas Sequence, southern Brazil. Sedimentary Geology, v. 92, p. 197-228.

De Ros, L.F., S. Morad, C. Broman, P. De Césero and D. Gomez-Gras 2000. Influence of uplift and magmatism on distribution of quartz and illite cementation: Evidence from Siluro-Devonian sandstones of the Paraná Basin, Brazil. International Association of Sedimentologists Special Publication no. 29, p. 231-252.

Dickinson, W.R., L.S. Beard, G.R. Brakenridge, J.L. Eriavec, R. Ferguson, K.F. Inman, R.A. Knepp, F.A. Lindberg and P.T. Ryberg 1983. Provenance of North America Phanerozoic sandstones in relation to tectonic setting. Geological Society of America Bulletin, v. 94, p. 222-235.

Dixon, S.A., D.M. Summers and R.C. Surdam 1989. Diagenesis and preservation of porosity in Norphlet Formation (Upper Jurassic), southern Alabama. American Association of Petroleum Geologists Bulletin, v. 73, p. 707-728.

Dworkin, S.I. and L.S. Land 1994. Petrographic and geochemical constraints on the formation and diagenesis of anhydrite cements, Smackover sandstones, Gulf of Mexico. Journal of Sedimentary Petrology, v. 64, p. 339-348.

Ehrenberg, S.N. 1991. Kaolinized, potassium-leached zones in the contacts of the Garn Formation, Haltenbanken, Mid-Norwegian Continental Shelf. Marine and Petroleum Geology, v. 8, p. 250-269.

Ehrenberg, S.N. 1993. Preservation of anomalously high porosity in deeply buried sandstones by grain-coating chlorite: Examples from the Norwegian Continental Shelf. American Association of Petroleum Geologists Bulletin, v. 77, p. 1260-1286.

El-Alami, M.A. 1996. Habitat of oil in Abu Attifel Area, Sirt Basin, Libya. In M.J. Salem, A.S. El-Hawat and A.M. Sbeta (Eds.), The Geology of Sirt Basin. Elsevier, Amsterdam, v. 2, p. 337-348.

Evans, I.J. 1989. Geochemical fluxes during shale diagenesis, an example from the Ordovician of Morocco. In D.L. Miles (Ed.), Water-rock Interaction WR1-6. Proceedings of the 6th International Symposium of Water-Rock Interaction, p. 219-222.

Finetti, I. 1982. Structure, stratigraphy and evolution of central Mediterranean. Bollettino di Gefisica Teorica and Applicata, v. 24, p. 247-312.

Fisher, Q.J., M. Casey, S.D. Harris and R.J. Knipe 2003. Fluid-flow properties of faults in sandstone: The importance of temperature history. Geology, v. 31, p. 965-968.

French, M.W, R.H. Worden, E. Mariani, R.E. Larese, R.R. Mueller and C.E. Kliewer 2012. Microcrystalline quartz generation and the preservation of porosity in sandstones: Evidence from the Upper Cretaceous of the Sub-Hercynian Basin, Germany. Journal of Sedimentary Research, v. 82, p. 422-434.

Friedman, I. and J.R. O'Neil 1977. Compilation of stable fractionation factors of geochemical interest. In M. Fleischer (Ed.), Data of Geochemistry. United States Geological Survey, Professional Paper 440-KK, 12 p.

Futyan, A. and A.H. Jawzi 1996. The hydrocarbon habitat of the oil and gas fields of North Africa with emphasis on the Sirt Basin. In M.J. Salem, A.S. El-Hawat and A.M. Sbeta (Eds.), The Geology of the Sirt Basin. Elsevier, Amsterdam, v. 2, p. 287-308.

Gaupp, R., A. Matter, J. Platt, K. Ramseyer and J. Walzebuck 1993. Diagenesis and fluid evolution of deeply buried Permian (Rotliegende) gas reservoirs, northwest Germany. American Association of Petroleum Geologists Bulletin, v. 77, p. 1111-1128.

Giles, M.R., S. Stevenson, S.V. Martin, S.J.C. Cannon, P.J. Hamilton, J.D. Marshall and G.M. Samways 1992. The reservoir properties and diagenesis of the Brent Group: A regional prospective. In A.C. Morton, R.S. Haszeldine, M.R. Giles and S. Brown (Eds.), Geology of the Brent Group. Geological Society of London Special Publication no. 61, p. 289-327.

Giles, M.R., S.L. Indrelid, G.V. Beynon and J. Amthor 2000. The origin of large-scale quartz cementation: Evidence from large data set and coupled heat-fluid mass transport modeling. In R.H. Worden and S. Morad (Eds.), Quartz Cementation in Sandstones. International Association of Sedimentologists Special Publication no. 29, Blackwell Science, Oxford, p. 21-38.

Glassman, J.R. 1992. The fate of feldspar in Brent Group reservoirs, North Sea: A regional synthesis of diagenesis in shallow, intermediate and deep burial environments. In A.C. Morton, R.S. Haszeldine, M.R. Giles and S. Brown (Eds.), Geology of the Brent Group. Geological Society of London Special Publication no. 61, p. 329-350.

Gluyas, J., L. Jolley and T. Primmer 1997. Element mobility during diagenesis: Sulphate cementation of Rotliegende sandstones, Southern North Sea. Marine and Petroleum Geology, v. 14, p. 1001-1011.

Goldstein, R.H. and T.G. Reynolds 1994. Systematics of fluid inclusions in diagenetic minerals. Society for Sedimentary Geology, Short Course, v. 31, 199 p.

Guiraud, R. and W. Bosworth 1997. Senonian Basin invasion and rejuvenation of rifting in Africa and Arabia: Synthesis and implication to plate-scale tectonics. Tectonophysics, v. 282, no. 1-4, p. 39-82.

Gumati, Y.D. and S. Schamel 1988. Thermal maturation history of the Sirt Basin, Libya. Journal of Petroleum Geology, v. 11, no. 2, p. 205-218.

Gumati, Y.D., W.H. Kanes and S. Schamel 1996. An evaluation of the hydrocarbon potential of the sedimentary basins of Libya. Journal of Petroleum Geology, v. 19, no. 1, p. 95-112.

Hallett, D. 2002. Petroleum Geology of Libya. Elsevier Science, Amsterdam, 502 p.

Hallett, D. and A. El-Ghoul 1996. Oil and gas potential of the deep through areas in the Sirt Basin. In M.J. Salem, A.S. El-Hawat and A.M. Sbeta (Eds.), The Geology of Sirt Basin. Elsevier, Amsterdam, v. 2, p. 455-484.

Hanor, J.S. 1994. Origin of saline fluids in sedimentary basins. In J. Parnell (Ed.), Geofluids: Origin, migration and evolution of fluids in sedimentary basins. Geological Society of London Special Publication no. 78, p. 151-174.

Harding, T.P. 1984. Graben hydrocarbon occurrence and structural style. American Association of Petroleum Geologists Bulletin, v. 68, p. 333-362.

Harwood, G. 1988. Microscopic techniques: II. Principles of sedimentary petrography. In M. Tucker (Ed.), Techniques in Sedimentology. Blackwell Scientific Publications, Oxford, p. 108-173.

Haszeldine, R.S., I.M. Samson and C. Cornford 1984. Quartz diagenesis and convective fluid movement; Beatrice Oilfield, UK North Sea. Clay Minerals, v. 19, p. 391-402.

Hendry, J.P., M. Wilkinson, A.E. Fallick and R.S. Haszeldine 2000. Ankerite cementation in deeply buried Jurassic sandstone reservoirs of the Central North Sea. Journal of Sedimentary Research, v. 70, no. 1, p. 227-239.

Hillier, S. 2003. Quantitative analysis of clay and other minerals in sandstones by X-ray powder diffraction (XRPD). In R.H. Worden and S. Morad (Eds.), Clay Mineral Cements in Sandstones. International Association of Sedimentologists Special Publication no. 34, Blackwell, Oxford, p. 213-251.

Hower, J., E.V. Eslinger, M.E. Hower and E.A. Perry 1976. Mechanism of burial metamorphism of argillaceous sediments: Part 1. Mineralogical and chemical evidence. Geological Society of America Bulletin, v. 87, p. 725-737.

Hurst, A. and H. Irwin 1982. Geological modeling of clay diagenesis in sandstones. Clays and Clay Minerals, v. 17, p. 5-22.

Khalifa, M. and S. Morad 2012. Impact of structural setting on diagenesis of fluvial and tidal sandstones: The Bahi Formation, Upper Cretaceous, NW Sirt Basin, North Central Libya. Marine and Petroleum Geology, v. 38, p. 211-231.

Knipe, R. 1993. The influence of fault zone processes and diagenesis on fluid flow. In A.D. Horbury and A.G. Robinson (Eds.), Diagenesis and Basin Development. American Association of Petroleum Geologists Studies in Geology, v. 36, p. 135-154.

Küpeli, S., M.M. Karadaĝ, A. Ayhan, A. Döyen and F. Arik 2007. C, O, Sr isotope studies on the genesis of Fe-carbonate and barite mineralization in the Attepe Iron District (Adana, Southern Turkey). Chemie der Erde Geochemistry, v. 67, no. 4, p. 313-322.

Land, L.S. and R.S. Fisher 1987. Wilcox sandstones diagenesis, Texas Gulf Coast: A regional isotopic comparison with the Frio Formation. In J.D. Marshall (Ed.), Diagenesis of Sedimentary Sequences. Geological Society of London Special Publication no. 36, p. 219-235.

Land, L.S., L.E. Mack, K.L. Milliken and F.L. Lynch 1997. Burial diagenesis of argillaceous sediments, south Texas Gulf of Mexico sedimentary basin: A reexamination. Geological Society of America Bulletin, v. 109, p. 2-15.

Magoon, L.B. and W.G. Dow 1994. The petroleum system from source to trap. American Association of Petroleum Geologists Memoir 60, p. 3-24.

McBride, E.F. 1963. A classification of common sandstone. Journal of Sedimentary Petrology, v. 33, p. 664-669.

Milliken, K.L., L.E. Mack and L.S. Land 1994. Elemental mobility in sandstones during burial: Whole-rock chemical and isotopic data, Frio Formation, south Texas. Journal of Sedimentary Research, v. 64, p. 788-796.

Morad, S. 1998. Carbonate cementation in sandstones: Distribution patterns and geochemical evolution. In S. Morad (Ed.), Carbonate Cementation in Sandstones. International Association of Sedimentologists Special Publication no. 26, Blackwell Science, Oxford, p. 1-26.

Morad, S., H. Ben Ismail, L.F. De Ros, I.S. Al-Aasm and N.E. Serrhini 1994. Diagenesis and formation water chemistry of Triassic reservoir sandstones from southern Tunisia. Sedimentology, v. 41, p. 1253-1272.

Morad, S., J.M. Ketzer and L.F. De Ros 2000. Spatial and temporal distribution of diagenetic alterations in siliciclastic rocks: Implications for mass transfer in sedimentary basins. Sedimentology, v. 47, Supplement 1, p. 95-120.

Morad, S., K. Al-Ramadan, J.M. Ketzer and L.F. De Ros 2010. The impact of diagenesis on the heterogeneity of sandstone reservoirs: A review of the depositional facies and sequence stratigraphy. American Association of Petroleum Geologists Bulletin, v. 94, p. 1267-1309.

Morley, C.K., R.A. Nelson, T.L. Patton and S.G. Munn 1990. Transfer zones in the East African rift system and their relevance to hydrocarbon exploration in the rifts. American Association of Petroleum Geologists Bulletin, v. 74, p. 1234-1253.

Ochoa, M., J. Arribas, R. Mas and R.H. Goldstein 2007. Destruction of a fluvial reservoir by hydrothermal activity (Cameros Basin, Spain). Sedimentary Geology, v. 202, p. 158-173.

Oelkers, E.H., P.A. Bjørkum and W.M. Murphy 1996. A petrographic and computational investigation of quartz cementation and porosity reduction in North Sea sandstones. American Journal of Science, v. 296, p. 420-452.

Petroconsultants 1996. Petroleum exploration and production database as of January, 1996. Petroconsultants, Inc., P.O. Box 740619, 6600. Sands Point Drive, Houston, TX 77274-0619, USA.

Pittman, E.D., R.E. Larese and M.T. Heald 1992. Clay coats: Occurrence and relevance to preservation of porosity in sandstones. In D.W. Houseknecht and E.D. Pittman (Eds.), Origin, diagenesis, and petrophysics of clay minerals in sandstones. Society of Economic Paleontologists and Mineralogists Special Publication, v. 47, p. 241-255.

Price, L.C. 1980. Utilization and documentation of vertical oil migration in deep basins. Journal of Petroleum Geology, v. 2, p. 353-387.

Robinson, G.R. Jr. 1992. Tectonic development of the base-metal and barite-vein deposits associated with the early Mesozoic basins of the eastern North America. In M.J. Bartholomew, D.W. Hyndman, D. Mogk and R. Mason (Eds.), Characterization and comparison of ancient and Mesozoic Continental margins. International Basement Tectonics Association Publication no. 8, Proceedings of the 8th International Conference on Basement and Tectonics, v. 2, p. 711-725.

Rossi, C., R. Marfil, K. Ramseyer and A. Permanyer 2001. Facies related diagenesis and multiphase siderite cementation and dissolution in the reservoir sandstones of the Khataba Formation, Egypt's Western Desert. Journal of Sedimentary Research, v. 71, p. 459-472.

Rossi, C., O. Kälin, J. Arribas and A. Tortosa 2002. Diagenesis, provenance and reservoir quality of Triassic TAGI sandstones from Ourhoud Field, Berkine (Ghadames) Basin, Algeria. Marine and Petroleum Geology, v. 19, p. 117-142.

Schröter, T. 1996. Tectonic and sedimentary development of the central Zallah Trough (West Sirt Basin, Libya). In M.J. Salem, M.T. Busrewil, A.A. Misallati and M.J. Sola (Eds.), Geology of the Sirt Basin. Elsevier, Amsterdam, v. 3, p. 123-136.

Sghair, A.M. 1996. Petrography, diagenesis and provenance of the Bahi Formation in the western part of the Sirt Basin, Libya. In M.J. Salam, A.S. El-Hawat and A.M. Sbeta (Eds.), The Geology of Sirt Basin. Elsevier, Amsterdam, v. 2, p. 65-82.

Sinha, R.N. and I.Y. Mriheel 1996. Evolution of subsurface Palaeocene sequence and shoal carbonates, south-central Sirt Basin. In M.J. Salam, A.S. El-Hawat and A.M. Sbeta (Eds.), The Geology of Sirt Basin. Elsevier, Amsterdam, v. 2, p. 153-195.

Starkey, H.C., P.D. Blackmon and P.L. Hauff 1984. The routine mineralogical analysis of clay-bearing samples. United States Geological Survey Bulletin 1563, 32 p.

Sullivan, M.D., R.S. Haszeldine and A.E. Fallick 1990. Linear coupling of carbon and strontium isotopes in Rotliegend Sandstone, North Sea: Evidence of cross-formational fluid flow. Geology, v. 18, p. 1215-1218.

Sullivan, M.D., R.S. Haszeldine, A.J. Boyce, G. Rogers and A.E. Fallick 1994. Late anhydrite cements mark basin inversion, isotopic and formation water evidence, Rotliegend Sandstone, North Sea. Marine and Petroleum Geology, v. 11, p. 46-54.

Thyne, G. 2001. A model for diagenetic mass transfer between adjacent sandstone and shale. Marine and Petroleum Geology, v. 18, p. 743-755.

Van der Meer, F. and S. Cloetingh 1996. Intraplate stress and the subsidence history of the Sirt Basin. In M.J. Salem, M.T. Busrewil, A.A. Misallati and M.A. Sola (Eds.), The Geology of Sirt Basin. Elsevier, Amsterdam, v. 3, p. 211-230.

Van der Plas, L. and A.C. Tobi 1965. A chart for judging the reliability of point counting results. American Journal of Science, v. 263, p. 87-90.

Van Houten, F.B. 1980. Latest Jurassic-Early Cretaceous regressive facies, northeast Africa Craton. American Association of Petroleum Geologists Bulletin, v. 64, p. 857-867.

Van Houten, F.B. 1983. Sirte Basin, north central Libya. Cretaceous rifting over a fixed mantle hotspot? Geology, v. 11, p. 115-118.

Walderhaug, O. 2000. Modeling quartz cementation and porosity in Middle Jurassic Brent Group sandstones of the Kvitebjørn Field, Northern North Sea. American Association of Petroleum Geologists Bulletin, v. 84, p. 1225-1339.

Wender, L.F., J.W. Bryant, M.F. Dickens, A.S. Neville and A.M. Al-Moqbel 1998. Paleozoic (pre-Khuff) hydrocarbon geology of the Ghawar area, eastern Saudi Arabia. GeoArabia, v. 3, no. 2, p. 273-302.

Wendte, J., I. Al-Aasm, G. Chi and D. Sargent 2009. Fault/fracture controlled hydrothermal dolomitization and associated diagenesis of the Upper Devonian Jean Marie member (Redknife Formation) in the July lake area of the Northeastern British Columbia. Bulletin of Canadian Petroleum Geology, v. 57, p. 275-322.

Worden, R.H. and S.A. Barclay 2000. Internal sourced quartz cement due to external derived CO2 in sub-arkosic sandstones, Northern North Sea, UKCS. Journal of Geochemical Exploration, v. 69-70, p. 645-694.

Worden, R.H. and S.D. Burly 2003. Sandstone diagenesis: the evolution of sand to stone. In S.D. Burley and R.H. Worden (Eds.), Sandstone Diagenesis: Recent and Ancient. International Association of Sedimentologists Special Publication no. 4, Blackwell, Oxford, p. 3-44.

Worden, R.H. and S. Morad 2000. Quartz cementation in oil field sandstones: A review of the key controversies. In R.H. Worden and S. Morad (Eds.), Quartz Cementation in Sandstones. International Association of Sedimentologists Special Publication no. 29, Blackwell Science, Oxford, p. 1-20.

Worden, R.H. and S. Morad 2003. Clay minerals in sandstones: Controls on formation, distribution and evolution. In R.H. Warden and S. Morad (Eds.), Clay Mineral Cements in Sandstones. International Association of Sedimentologists Special Publication no. 34, Blackwell, Oxford, p. 3-41.

Worden, R.H., N.H. Oxtoby and P.C. Smalley 1998. Can oil emplacement prevent quartz cementation in sandstones? Petroleum Geosciences, v. 4, p. 129-139.

Worden, R.H., M.W. French and E. Mariani 2012. Amorphous silica nanofilms result in growth of misoriented microcrystalline quartz cement maintaining porosity in deep buried sandstones. Geology, v. 40, no. 2, p. 179-182.

ABOUT THE AUTHORS

Muftah Khalifa *obtained his BSc degree in Geology from the Higher Petroleum Institute, Tubrok (Libya) in 1980, and MPhil degree in Sedimentology from Manchester University, UK in 1997. From 1980 to 2001 he worked as Geologist with AGIP and Waha Oil Company, Libya. He joined the Engineering department/Reservoir study division, Libyan Petroleum Institute, Tripoli (Libya) in 2001 as a Sedimentologist/Assistant Researcher. He published one paper in the Marine and Petroleum Geology Journal and two papers in the Libyan Petroleum Institute Journal about diagenesis of Cretaceous sandstones. His current research deals with the impact of diagenesis on siliciclastic reservoirs.*

akhmuftah@yahoo.com

Marta Gasparrini *joined IFP Energies nouvelles in 2009. She obtained her PhD in Geology from the University of Heidelberg in Germany (2003). She also worked as Research-Sedimentologist for the University of Naples, Italy and the INGV – National Institute for Geophysics and Volcanology, Italy. She mainly addressed her research into developing conceptual models in diagenesis and hydrothermal alteration of carbonates.*

marta.gasparrini@ifpen.fr

Manuscript submitted July 7, 2013

Revised February 11, 2014

Accepted March 27, 2014